Modelling error distribution in the ground reaction force during an induced-acceleration analysis of running in rear-foot strikers

SEKIYA KOIKE[1], SEIGO NAKAYA[2], HIROTO MORI[2], TATSUYA ISHIKAWA[2], & ALEXANDER P. WILLMOTT[3]

[1]*Faculty of Health and Sport Sciences, University of Tsukuba, Japan,* [2]*Institute of Sport Science, Asics Corporation, Japan, and* [3]*School of Sport and Exercise Science, University of Lincoln, UK*

Running Title: Modelling error distribution in the GRF in running

Corresponding Author:

Sekiya Koike, Faculty of Health and Sport Sciences, University of Tsukuba, Japan.

Tel: +81 – 29 – 853 – 2677 Email: koike.sekiya.fp@u.tsukuba.ac.jp

Other Authors:

Seigo Nakaya, Institute of Sport Science, Asics Corporation, Japan.

Tel: +81 – 78 – 992 – 0810 Email: seigo.nakaya@asics.com

Hiroto Mori, Institute of Sport Science, Asics Corporation, Japan.

Tel: +81 –78 – 992 – 0810 Email: hiroto.mori@asics.com

Tatsuya Ishikawa, Institute of Sport Science, Asics Corporation, Japan.

Tel: +81 – 78 – 992 – 0810 Email: tatsuya.ishikawa@asics.com

Alexander Peter Willmott, School of Sport and Exercise Science, University of Lincoln, UK.

Tel: +44 – 1522 – 886651 Email: swillmott@lincoln.ac.uk

Acknowledgements:

This work was supported by JSPS KAKENHI under Grant Number JP24500726.

Word Count: 4745

Abstract

The objective of this study was to develop and evaluate a methodology for quantifying the contributions of modelling error terms, as well as individual joint torque, gravitational force and motion-dependent terms, to the generation of ground reaction force (GRF), whose true value can be measured with high accuracy using a force platform. Dynamic contributions to the GRF were derived from the combination of 1) the equations of motion for the individual segments, 2) the equations for constraint conditions arising from the connection of adjacent segments at joints, and 3) the equations for anatomical constraint axes at certain joints. The contribution of the error term was divided into four components caused by fluctuation of segment lengths, geometric variation in the constraint joint axes, and residual joint force and moment errors. The proposed methodology was applied to the running motion of thirteen rear-foot strikers at a constant speed of 3.3 m/s. Modelling errors arose primarily from fluctuations in support leg segment lengths and rapid movement of the virtual joint between the foot and ground during the first 20% of stance phase. The magnitudes of these error contributions to the vertical and anterior/posterior components of the GRF are presented alongside the non-error contributions, of which the joint torque term was the largest.

Keywords: dynamic contribution, induced-acceleration analysis, modelling error, running, ground reaction force

Introduction

Human movement, which can feature high velocity and acceleration of a whole body or parts of one, is mainly driven by joint torques originating in muscle contractions. Since a human body consists of segments connecting at joints, the inertial matrix of the equation of motion for the system is non-diagonal and therefore a torque input about one joint axis can cause multi-axial angular accelerations of the body. This phenomenon is called dynamic coupling (Kane & Levinson, 1985). Human movement is determined by equations of motion that describe causal relationships between input variables (e.g. joint torques) and output variables (e.g. horizontal and vertical accelerations of the whole-body's centre of gravity). If the accelerations of relevant body parts are known then the equations of motion can be used to derive the dynamic relationship between joint torques and the observed movements. Induced-acceleration analysis of this type has been demonstrated to be highly effective for quantifying the joint torque or muscle force contributions to biomechanical quantities such as the velocity and acceleration of the whole-body centre of gravity or end-point speed in complex multi-joint sports motions such as running (Putnam, 1991; Sasaki & Neptune, 2006; Hamner et al., 2010; Hamner et al., 2013), jumping (Koike et al., 2007), throwing (Putnam, 1993; Hirashima et al., 2008; Naito and Maruyama, 2008), kicking (Putnam, 1991; Putnam, 1993) and pedalling (Fregly & Zajac, 1996).

Errors will, however, be generated during any induced-acceleration analysis that calculates the contribution of joint torques to body movements. Despite the fact that each segment of the human body consists of both rigid and soft-structure components, the body is usually modelled for simplicity as a set of linked rigid segments. Nominal values for body segment parameters such as length, mass and inertia are used in the analysis of sports motion, but the mechanical properties of the human body are not known precisely enough to allow for detailed modelling (Gruber et al., 1998). For example, during an impact such as a heel strike in running the impact force causes rapid accelerations of the body, and soft tissue structures ("wobbling mass") may move with respect to the rigid part of the associated segment. The impact forces can also cause motion artefacts in markers attached to the skin. Limitations

therefore inevitably arise during an induced-acceleration analysis based on a human body model consisting of linked rigid segments. Although a Residual Reduction Algorithm that modifies the observed motion data has been proposed in order to reduce errors in ground reaction force during dynamic simulation (Delp et al., 2007), the contribution of modelling errors is not included in the analysis.

While estimating the magnitude of modelling errors is necessary for appropriate evaluation of the contributions from individual joint torques, the influences that specific errors have on the contributions of joint torques have never been demonstrated. Restrictions on the consideration of modelling errors can occur when joint or segment angles are selected as the generalized variables in deriving the equation of motion for the target system. Several previous induced-acceleration analyses have employed a Kane's method or Newton-Euler method approach using joint angular displacements as generalized variables (Zajac et al., 2002, 2003; Hirashima et al., 2008; Naito & Maruyama, 2008), but residual errors were not taken into account when deriving the equations of motion because to do so would make the analysis more complex due to the increased number of variables necessary for expression of the state of the system. It would thus become difficult to quantify the contribution of modelling errors to the generation of biomechanical quantities.

The objective of this study was to estimate the contributions from different sources of modelling error to ground reaction force values calculated using an induced-acceleration approach. The contribution of the error term to the ground reaction force can be divided into component terms arising from changes in segment lengths, geometric variation in the anatomical constraint joint axes, and residual errors in joint force and moment mainly due to errors in the body segment parameters. The proposed methodology was applied to the running motion at constant speed of rear-foot strikers. Developing methods for quantifying the contributions of modelling errors will complement existing methods for analysing the contribution of joint torques to whole body motion and aid investigation of the biomechanics of human movement.

Methods

In order to quantify the contribution of modelling errors in an induced-acceleration analysis, a methodology is proposed that derives an analytical model by coupling four types of equations: 1) equations of motion for each individual segment within the target system, 2) geometric constraint equations resulting from the connection of adjacent segments by joints, 3) joint constraint equations arising from consideration of the anatomical degrees of freedom for axes such as the varus /valgus axis at the knee and elbow joints, and 4) moment distribution equations which divide joint moment vectors into separate active and constraint joint torque vectors.

Figure 1 shows a schematic diagram of a whole-body model containing 15 rigid segments. The segments are classified into five groups: right upper limb, left upper limb, right lower limb, left lower limb, and head and trunk segments. Each group has an identification number, *k*, between one and five (as shown in the figure) and comprises three segments. The right lower limb is assumed to connect with the ground via a virtual joint at the centre of pressure (COP) of the right foot.

****Figure 1 near here****

Whole-body dynamical model

Under the assumption that the human body can be modelled as a set of linked segments, the equations of motion for the linear and angular motion of segment *k,i*, as shown by Figure 2, can be written as:

****Figure 2 near here****

$$m_{k,i}\ddot{\boldsymbol{x}}_{k,i} = \boldsymbol{f}_{k,j} - \boldsymbol{f}_{k,j+1} + m_{k,i}\boldsymbol{g} \tag{1}$$

$$\hat{\boldsymbol{I}}_{k,i}\dot{\boldsymbol{\omega}}_{k,i} + \boldsymbol{\omega}_{k,i} \times \left(\hat{\boldsymbol{I}}_{k,i}\boldsymbol{\omega}_{k,i}\right) = \boldsymbol{r}_{k,i,\overline{\text{cg-P}}} \times \boldsymbol{f}_{k,j} - \boldsymbol{r}_{k,i,\overline{\text{cg-D}}} \times \boldsymbol{f}_{k,j+1} + \boldsymbol{n}_{k,j} - \boldsymbol{n}_{k,j+1} \tag{2}$$

where $m_{k,i}$ is the mass of the segment, $\boldsymbol{x}_{k,i}$ is the position vector of the segment's centre of

gravity (CG), $\boldsymbol{f}_{\_k,j}$ is the joint force vector applied at the *k*,*j*-th joint by the more proximal segment to the more distal one, $\boldsymbol{g}$ is the gravitational acceleration vector, $\hat{\boldsymbol{I}}_{k,i}$ is the inertia matrix of the segment expressed in the global reference coordinate system, and $\boldsymbol{\omega}_{k,i}$ is the angular velocity vector for the segment. The vectors $\boldsymbol{r}_{k,i}$ with barred subscripts cg-P and cg-D denote position vectors running from the CG of the segment to the proximal and distal endpoints of the segment, respectively. The vector $\boldsymbol{n}_{k,j}$ is the moment vector applied about the *k*,*j*-th joint by the more proximal segment to the more distal one, which is calculated from inverse dynamics computations.

The equations for the foot segment in direct contact with the ground during the support phase are as follows:

$$m_{3,3}\ddot{\boldsymbol{x}}_{3,3} = m_{3,3}\boldsymbol{g} + \boldsymbol{f}_{3,3} - \boldsymbol{f}_{\mathrm{COP}} \tag{3}$$

$$\hat{\boldsymbol{I}}_{3,3}\dot{\boldsymbol{\omega}}_{3,3} + \boldsymbol{\omega}_{3,3} \times \left(\hat{\boldsymbol{I}}_{3,3}\boldsymbol{\omega}_{3,3}\right) = \boldsymbol{r}_{3,3,\overline{\mathrm{cg\text{-}P}}} \times \boldsymbol{f}_{3,3} + \boldsymbol{r}_{3,3,\overline{\mathrm{cg\text{-}D}}} \times \boldsymbol{f}_{\mathrm{COP}} + \boldsymbol{n}_{3,3} - \boldsymbol{n}_{\mathrm{COP}} \tag{4}$$

where subscript 3,3 denotes the right foot segment, and the subscript COP denotes the centre of pressure at the contact point on the ground. $\boldsymbol{f}_{\mathrm{COP}}$ and $\boldsymbol{n}_{\mathrm{COP}}$ denote the ground reaction force and free moment vectors, respectively, acting on the foot; they were measured with a force platform.

In order to deal with modelling errors mainly caused by body segment parameter errors, which are inevitable when modelling the human body, residual error compensation force and moment vectors, $\boldsymbol{f}_{\mathrm{r}}$ and $\boldsymbol{n}_{\mathrm{r}}$, acting at the top of head segment are introduced. The equations of translational and rotational motion for the head segment are written as follows:

$$m_{5,1}\ddot{\boldsymbol{x}}_{5,1} = m_{5,1}\boldsymbol{g} + \boldsymbol{f}_{5,1} + \boldsymbol{f}_{\mathrm{r}} \tag{5}$$

$$\hat{\boldsymbol{I}}_{5,1}\dot{\boldsymbol{\omega}}_{5,1} + \boldsymbol{\omega}_{5,1} \times \left(\hat{\boldsymbol{I}}_{5,1}\boldsymbol{\omega}_{5,1}\right) = \boldsymbol{r}_{5,1,\overline{\mathrm{cg\text{-}P}}} \times \boldsymbol{f}_{5,1} + \boldsymbol{r}_{5,1,\overline{\mathrm{cg\text{-}D}}} \times \boldsymbol{f}_{\mathrm{r}} + \boldsymbol{n}_{5,1} + \boldsymbol{n}_{\mathrm{r}} \tag{6}$$

where $\boldsymbol{f}_{\mathrm{r}}$ and $\boldsymbol{n}_{\mathrm{r}}$ were obtained via inverse dynamics calculations that started from the support foot and the ground reaction force measured with the force platform.

The dynamical equations for individual segments can be expressed in a matrix form with respect to all segments as follows (see Appendix 1 for more detail):

$$\boldsymbol{M}\dot{\boldsymbol{V}} = \boldsymbol{PF} + \boldsymbol{QN} + \boldsymbol{P}_r \boldsymbol{f}_r + \boldsymbol{Q}_r \boldsymbol{n}_r + \boldsymbol{H} + \boldsymbol{G} \tag{7}$$

where $\boldsymbol{M}$ is the inertia matrix, and $\boldsymbol{V}$ is the generalized velocity vector consisting of linear velocity vectors and angular velocity vectors for all the segments. $\boldsymbol{P}$ is the coefficient matrix for vector $\boldsymbol{F}$ which contains all joint force vectors and the ground reaction force vector $\boldsymbol{f}_{\mathrm{COP}}$. $\boldsymbol{Q}$ is the coefficient matrix for vector $\boldsymbol{N}$ which contains all joint moment vectors and the ground reaction free moment vector $\boldsymbol{n}_{\mathrm{COP}}$. $\boldsymbol{H}$ is the gyroscopic moment vector, and $\boldsymbol{G}$ is the vector due to the gravitational force. $\boldsymbol{P}_{\mathrm{r}}$ and $\boldsymbol{Q}_{\mathrm{r}}$ are the coefficient matrices for the compensation vectors $\boldsymbol{f}_{\mathrm{r}}$ and $\boldsymbol{n}_{\mathrm{r}}$.

Assuming that every segment is connected to its adjacent segment at a joint, the geometric constraint for linked segments can be expressed as:

$$\boldsymbol{x}_{k,i} + \boldsymbol{r}_{k,i,\overline{\text{cg-D}}} - \boldsymbol{x}_{k,i+1} - \boldsymbol{r}_{k,i+1,\overline{\text{cg-P}}} = \boldsymbol{O}_{3\times1} \tag{8}$$

where $\boldsymbol{O}_{3\text{x}1}$ is a zero matrix with three rows and one column. Additionally, in the case of motion with the foot contacting the ground, such as the support phase of running or walking, the ground-contact constraint can be obtained using the assumption that the foot segment of the support leg is connected with the ground at the COP by a virtual joint:

$$\boldsymbol{x}_{3,3} + \boldsymbol{r}_{3,3,\overline{\text{cg-CP}}} = \boldsymbol{x}_{\mathrm{COP}} \tag{9}$$

Differentiating each segment's geometric constraint equation (Equation 8) once with respect to time yields:

$$\dot{\boldsymbol{x}}_{k,i} + \boldsymbol{\omega}_{k,i} \times \boldsymbol{r}_{k,i,\overline{\text{cg-D}}} + \dot{\boldsymbol{r}}^{*}_{k,i,\overline{\text{cg-D}}} - \dot{\boldsymbol{x}}_{k,i+1} - \boldsymbol{\omega}_{k,i+1} \times \boldsymbol{r}_{k,i+1,\overline{\text{cg-P}}} - \dot{\boldsymbol{r}}^{*}_{k,i+1,\overline{\text{cg-P}}} = \boldsymbol{O}_{3\times1} \tag{10}$$

where vectors $\dot{\boldsymbol{r}}^{*}_{\underline{k},i}$ with barred subscripts cg-D and cg-P represent velocity vectors, expressed in the $\underline{k},i$-th segment coordinate system, arising from fluctuations in the lengths of the position vectors from the segment's CG to its distal and proximal ends, respectively. The constraint equation for all joints can be represented in matrix form as:

$$\boldsymbol{CV} = \dot{\boldsymbol{\eta}} \tag{11}$$

where $\boldsymbol{C}$ is the coefficient matrix for vector $\boldsymbol{V}$, and $\dot{\boldsymbol{\eta}}$ is the vector consisting of the differences between the distal and proximal point velocity vectors at individual joints (see

Appendix 2 for more detail).

The equations for the anatomical constraint axes (e.g. varus/valgus axis at elbow and knee joints), along which the joints cannot rotate freely, can be characterized as follows:

$$\boldsymbol{e}_{k,1,x}^{\mathrm{T}}\boldsymbol{e}_{k,2,z} = \varphi_{k,2}(t), \quad (k=1,2,3,4) \tag{12}$$

where $\boldsymbol{e}_{k,1,x}$ and $\boldsymbol{e}_{k,2,z}$ are unit vectors directed as shown in Figure 1, and $\varphi_{k,i}$(t) is the inner product of the two unit vectors. In the figure, segment 1 denotes the upper arm or thigh, and segment 2 denotes the adjacent forearm or shank. When these unit vectors are perpendicular to each other, $\varphi_{k,i}(t)$ equals zero (Fujii & Hubbard, 2002).

Differentiating the constraint equation once with respect to time yields a velocity constraint equation:

$$\boldsymbol{e}_{k,2,z}^{\mathrm{T}}\left(\boldsymbol{e}_{k,1,x}\times\boldsymbol{\omega}_{k,1}\right)+\boldsymbol{e}_{k,1,x}^{\mathrm{T}}\left(\boldsymbol{e}_{k,2,z}\times\boldsymbol{\omega}_{k,2}\right)=-\dot{\varphi}_{k,2}(t) \tag{13}$$

Differentiating all the anatomical constraint equations with respect to time yields a matrix form anatomical constraint equation:

$$\boldsymbol{A}\boldsymbol{V}=\dot{\boldsymbol{\varphi}} \tag{14}$$

where $\boldsymbol{A}$ is the coefficient matrix for vector $\boldsymbol{V}$ (see Appendix 3 for more detail).

The joint moment vector $\boldsymbol{N}$ can be considered to be the sum of an active joint torque vector $\boldsymbol{T}_{\mathrm{a}}$ and a constraint joint torque vector $\boldsymbol{T}_{\mathrm{p}}$:

$$\boldsymbol{N}=\boldsymbol{S}_{\mathrm{a}}\boldsymbol{T}_{\mathrm{a}}+\boldsymbol{S}_{\mathrm{p}}\boldsymbol{T}_{\mathrm{p}} \tag{15}$$

where the matrices $\boldsymbol{S}_{\mathrm{a}}$ and $\boldsymbol{S}_{\mathrm{p}}$ are the coefficient matrices for $\boldsymbol{T}_{\mathrm{a}}$ and $\boldsymbol{T}_{\mathrm{p}}$, respectively (see Appendix 4 for more detail).

Dynamic equation of joint force vector including ground reaction force

Differentiating Equations (11) and (14) with respect to time yields constraint equations:

$$\boldsymbol{C}\dot{\boldsymbol{V}}+\dot{\boldsymbol{C}}\boldsymbol{V}=\ddot{\boldsymbol{\eta}} \tag{16}$$

$$\boldsymbol{A}\dot{\boldsymbol{V}}+\dot{\boldsymbol{A}}\boldsymbol{V}=\ddot{\boldsymbol{\varphi}} \tag{17}$$

Substituting Equations (15), (16) and (17) into Equation (7) yields a dynamic equation for the

whole-body system as follows:

$$\begin{bmatrix} \dot{\boldsymbol{V}} \\ \boldsymbol{F} \\ \boldsymbol{T}_{\mathrm{p}} \end{bmatrix} = \begin{bmatrix} \boldsymbol{M} & -\boldsymbol{P} & -\boldsymbol{Q}\boldsymbol{S}_{\mathrm{p}} \\ \boldsymbol{C} & \boldsymbol{O}_{45\times45} & \boldsymbol{O}_{45\times8} \\ \boldsymbol{A} & \boldsymbol{O}_{8\times45} & \boldsymbol{O}_{8\times8} \end{bmatrix}^{-1} \left\{ \begin{bmatrix} \boldsymbol{Q}\boldsymbol{S}_{\mathrm{a}} \\ \boldsymbol{O} \\ \boldsymbol{O} \end{bmatrix} \boldsymbol{T}_{\mathrm{a}} + \begin{bmatrix} \boldsymbol{H} \\ -\dot{\boldsymbol{C}}\boldsymbol{V} \\ -\dot{\boldsymbol{A}}\boldsymbol{V} \end{bmatrix} + \begin{bmatrix} \boldsymbol{E} \\ \boldsymbol{O} \\ \boldsymbol{O} \end{bmatrix} \boldsymbol{G} + \begin{bmatrix} \boldsymbol{P}_r \\ \boldsymbol{O} \\ \boldsymbol{O} \end{bmatrix} \boldsymbol{f}_r + \begin{bmatrix} \boldsymbol{Q}_r \\ \boldsymbol{O} \\ \boldsymbol{O} \end{bmatrix} \boldsymbol{n}_r + \begin{bmatrix} \boldsymbol{O} \\ \boldsymbol{E} \\ \boldsymbol{O} \end{bmatrix} \ddot{\boldsymbol{\eta}} + \begin{bmatrix} \boldsymbol{O} \\ \boldsymbol{O} \\ \boldsymbol{E} \end{bmatrix} \ddot{\boldsymbol{\varphi}} \right\} \tag{18}$$

A dynamic equation for joint force vector $\boldsymbol{F}$, which includes the ground reaction force, can be obtained as follows:

$$\boldsymbol{F} = \boldsymbol{A}_{F,Ta}\boldsymbol{T}_{\mathrm{a}} + \boldsymbol{A}_{F,V} + \boldsymbol{A}_{F,G}\boldsymbol{G} + \boldsymbol{A}_{F,fr}\boldsymbol{f}_{\mathrm{r}} + \boldsymbol{A}_{F,nr}\boldsymbol{n}_{\mathrm{r}} + \boldsymbol{A}_{F,\eta}\ddot{\boldsymbol{\eta}} + \boldsymbol{A}_{F,\varphi}\ddot{\boldsymbol{\varphi}} \tag{19}$$

where $\boldsymbol{A}_{F,Ta}$ and $\boldsymbol{A}_{F,G}$ indicate coefficient matrices for the joint torque vector $\boldsymbol{T}_{\mathrm{a}}$ and gravitational force vector $\boldsymbol{G}$, $\boldsymbol{A}_{F,V}$ indicates the motion-dependent torque vector consisting of centripetal and Coriolis forces, $\boldsymbol{A}_{F,Fr}$ and $\boldsymbol{A}_{F,Nr}$ are coefficient matrices for the compensation force and moment inputs $\boldsymbol{f}_{\mathrm{r}}$ and $\boldsymbol{n}_{\mathrm{r}}$, and $\boldsymbol{A}_{F,\eta}$ and $\boldsymbol{A}_{F,\varphi}$ are coefficient matrices for the vectors $\ddot{\boldsymbol{\eta}}$ and $\ddot{\boldsymbol{\varphi}}$ (see Appendix 5 for more detail). The terms on the right-hand-side of Equation (19) represent in order the contribution of the joint moment term, motion-dependent term, gravitational term, compensational force term, compensational moment term, segment length fluctuation term, and constraint joint axial angle fluctuation term to the generation of joint force vector $\boldsymbol{F}$.

Contributions to the generation of ground reaction force

The ground reaction force $\boldsymbol{f}_{\mathrm{GRF}}$ can be extracted from the generalized joint force vector $\boldsymbol{F}$, which consists of all joint force vectors:

$$\boldsymbol{f}_{\mathrm{GRF}} = \boldsymbol{S}_{\mathrm{GRF}}\boldsymbol{F}, \quad \boldsymbol{S}_{\mathrm{GRF}} = \begin{bmatrix} \boldsymbol{O}_{3\times9} & \boldsymbol{O}_{3\times9} & \boldsymbol{O}_{3\times9} & -\boldsymbol{E} & \boldsymbol{O}_{3\times9} & \boldsymbol{O}_{3\times6} \end{bmatrix} \tag{20}$$

In turn, the ground reaction force vector can be broken down into its components as follows:

$$\boldsymbol{f}_{\mathrm{GRF}} = \boldsymbol{C}_{\mathrm{GRF},Ta} + \boldsymbol{C}_{\mathrm{GRF},V} + \boldsymbol{C}_{\mathrm{GRF},G} + \Delta\boldsymbol{C}_{\mathrm{GRF},err}, \quad \Delta\boldsymbol{C}_{\mathrm{GRF},err} = \boldsymbol{C}_{\mathrm{GRF},fr} + \boldsymbol{C}_{\mathrm{GRF},nr} + \boldsymbol{C}_{\mathrm{GRF},\eta} + \boldsymbol{C}_{\mathrm{GRF},\varphi} \tag{21}$$

where the terms $\boldsymbol{C}_{\mathrm{GRF},Ta}$, $\boldsymbol{C}_{\mathrm{GRF},V}$ and $\boldsymbol{C}_{\mathrm{GRF},G}$ indicate the contributions to the ground reaction force vector of the joint torque term, the motion-dependent term, and the gravity term respectively; and $\Delta\boldsymbol{C}_{\mathrm{GRF},err}$ is the residual error vector consisting of four terms: the residual force error term $\boldsymbol{C}_{\mathrm{GRF},Fr}$ and the residual moment error term $\boldsymbol{C}_{\mathrm{GRF},Nr}$ (with these two terms

arising from errors in body segment parameters), the segment length fluctuation term $\boldsymbol{C}_{\mathrm{GRF},\eta}$, and the joint anatomical constraint axes fluctuation term $\boldsymbol{C}_{\mathrm{GRF},\varphi}$.

In the inverse dynamics calculation, the GRF data are used to obtain static components of the joint torques via a static relationship between $\boldsymbol{F}_{\mathrm{GRF}}$ (the ground reaction force vector) and $\boldsymbol{T}_{\mathrm{a,sup}}$ (the support leg active joint torque vector) as follows:

$$\boldsymbol{T}_{\mathrm{a,sup}} = \boldsymbol{J}^{\mathrm{T}}\boldsymbol{F}_{\mathrm{GRF}} \tag{22}$$

where $\boldsymbol{J}$ is the Jacobian matrix consisting of the outer product matrices of position vectors pointing to the COP from the individual joint centres. Since the number of DOFs associated with $\boldsymbol{T}_{\mathrm{a,sup}}$ and $\boldsymbol{F}_{\mathrm{GRF}}$ are seven (three at the hip, two at each of the knee and ankle joints) and three (X, Y and Z in the global coordinate system), respectively, the dimensions of the transposed Jacobian matrix are seven by three. It is, therefore, impossible to obtain the magnitude of the contributions to the GRF from individual joint torques by using the inverse matrix of $\boldsymbol{J}^{\mathrm{T}}$ (i.e. $\boldsymbol{F}_{\mathrm{GRF}}=(\boldsymbol{J}^{\mathrm{T}})^{-1}\,\boldsymbol{T}_{\mathrm{a,sup}}$) because the inverse matrix of the Jacobian does not exist due to the singularity of that matrix. By contrast, in the analysis of dynamic contributions of individual joint torques to the GRF, it is possible to determine the magnitude of these individual contributions by using equations of motion for the whole body.

Data collection

Thirteen male participants (rear-foot strikers; age: 30.5 ± 6.1 years; height: 1.74 ± 0.03 m; body mass: 70.7 ± 7.5 kg) participated in this study. Written informed consent was given prior to their participation, and approval for the experiment was obtained from the institution's ethics committee. The participants were asked to run under a constant speed condition (3.3 m/s) after accelerating over a distance of 15 m. The running speed was measured using photo cells (IRD-T175, Brower Timing System, Utah, USA) set 5 m apart, and only trials within 3% of the speed condition were included in the analysis. It should be noted that no trials contained any periods of double support. Forty-seven reflective markers were attached to the

participant's body (Figure 3), as described in Suzuki et al. (2014), and their 3-dimensional coordinate data were captured with a motion capture system consisting of 16 infrared cameras (VICON-MX, Vicon Motion Systems Ltd., Oxford, UK). The proximal endpoint of the lower torso was defined as the mid-point of the markers affixed to the lower ends of the right and left ribs. One force platform (9287B, Kistler Inc., Winterthur, Switzerland) provided the ground reaction force (GRF) data that were required to calculate the net joint moment. The motion capture system and the force platform were synchronized with data being sampled at 250 Hz and 1000 Hz, respectively. The coordinate data were smoothed with a fourth-order zero-phase-shift Butterworth low-pass digital filter whose optimal cut-off frequencies were determined by the residual method (Wells & Winter, 1980) and ranged from 5 to 15 Hz. The signal outputs from the force platform were smoothed with a fourth-order zero-phase-shift Butterworth low-pass digital filter with constant cut-off frequency of 150 Hz. In addition, in order to reduce the high-frequency noise component of acceleration of the COP fluctuation at the virtual joint when calculating the second derivative of the fluctuation term, a fifth-order polynomial function whose coefficients were determined by a least-squares method with respect to residual position errors was applied to the COP coordinate data. Data from four trials per participant were analysed.

****Figure 3 near here****

The joint torques about the individual joint axes were calculated using the inverse dynamics approach. The contributions of the joint torque, motion-dependent torque term, gravitational term and residual modelling error terms to the generations of the ground reaction force were calculated from Equation (21). All times were normalised with respect to the percentage of the stance phase duration, and the contributions of individual terms were averaged across the participants at normalised times from 0 to 100% of the stance phase.

The influence of the choice of low-pass cut-off frequency for smoothing on the magnitude of the modelling error terms was investigated by quantifying the average contribution of each individual error term to the GRF over the duration of the stance phase, as

calculated by Equation (23). These contributions were determined for frequencies ranging from 5 to 50 Hz:

$$r_{\mathrm{Err,GRF},\,j,i}(C_{j,i}) = \frac{\int \left| C_{j,i}(t) \right| dt}{\int \left| \boldsymbol{f}_{\mathrm{GRF},i}(t) \right| dt} \times 100\,[\%], \quad (23)$$

$(i = \mathrm{v} : \text{vertical},\ i = \mathrm{a/p} : \text{anterior/posterior}),\ (C_j = C_{\mathrm{GRF},\,\boldsymbol{fr}}, C_{\mathrm{GRF},\boldsymbol{nr}}, C_{\mathrm{GRF},\boldsymbol{\eta}}, C_{\mathrm{GRF},\boldsymbol{\varphi}})$

The relative contributions of the total modelling error term (the sum of the four sources identified in Equation 23) and the three non-error terms to the GRF components were also calculated as a percentage across the whole phase:

$$r_{\mathrm{GRF},k,i}(C_{k,i}) = \frac{\int \left| C_{k,i}(t) \right| dt}{\int \left| \boldsymbol{f}_{\mathrm{GRF},i}(t) \right| dt} \times 100\,[\%], \quad (24)$$

$(i = \mathrm{v} : \text{vertical},\ i = \mathrm{a/p} : \text{anterior/posterior}),\ (C_k = C_{\mathrm{GRF},\boldsymbol{Ta}}, C_{\mathrm{GRF},\boldsymbol{V}}, C_{\mathrm{GRF},\boldsymbol{G}}, \Delta C_{\mathrm{GRF},\boldsymbol{err}})$

Similarly, the relative contribution of each individual error term to the total modelling error was calculated as a percentage across the whole phase:

$$r_{\mathrm{Error},\,j,i}(C_{j,i}) = \frac{\int \left| C_{j,i}(t) \right| dt}{\int \left\{ \left| C_{\mathrm{GRF},\,\boldsymbol{fr},i}(t) \right| + \left| C_{\mathrm{GRF},\boldsymbol{nr},i}(t) \right| + \left| C_{\mathrm{GRF},\boldsymbol{\eta},i}(t) \right| + \left| C_{\mathrm{GRF},\boldsymbol{\varphi},i}(t) \right| \right\} dt} \times 100\,[\%] \quad (25)$$

where $C_{j,i}$ and i are same as those in Equation (23).

Results

The sum of the individual contributions matched the measured vertical ground reaction force throughout the phase (Figure 4a). The joint torque term was the largest contributor to the vertical ground reaction force over the entire support duration (Figure 4b, 96.39 ± 0.72 % from Equation 24). The magnitude of the total modelling error term was largest, and showed greatest variability, during the first 20% of the phase (Figure 4e). By far the largest contribution to this term arose from fluctuations in segment lengths (Figure 5a, 85.20 ± 4.35% from Equation 25); the contributions from anatomical constraint axis fluctuations, the residual force and the residual moment were negligible (each less than 7 %; Figures 5b, c and d).

****Figure 4 near here****

****Figure 5 near here****

Similar findings were obtained when the contributions to the anterior/posterior ground reaction force were analysed. The sum of the contributions in this direction again matched the measured value (Figure 6a), with the joint torque term accounting for a large proportion of the total force throughout the entire stance phase (Figure 6b, 99.06 ± 2.95 %). The magnitude of the modelling error was again largest and most variable during the first 20% of the phase (Figure 6e), and it was also dominated by the component arising from fluctuations in segment lengths (Figure 7a, 85.45 ± 3.33 %). For individual participants the time histories of both the vertical and anterior/posterior modelling error components were highly conserved.

****Figure 6 near here****

****Figure 7 near here****

Exploring the sources of the segment length error further, Figures 8a and b show the detail of the contributions to the normalised vertical and anterior/posterior ground reaction forces, respectively, from the segment fluctuation terms at individual joints. The contributions associated with the support leg joints and the virtual joint at COP were large relative to those from the joints of the upper limbs and swing leg, and from the head and trunk.

****Figure 8 near here****

With the exception of the residual force and moment error terms when the cut-off frequency for smoothing was changed from 5 to 15 Hz, all of the error term contributions to the vertical components of the GRF increased in magnitude as the cut-off frequency was raised from 5 to 15 Hz, and then to 25 and 50 Hz (Table 1a). Similarly, with the exception of the residual force error

term when the cut-off frequency was changed from 5 to 15 Hz, the contribution to the anterior/posterior component of the GRF from each error term also increased with cut-off frequency (Table 1b). The average contribution to the GRF components over the stance phase remained below 1.5%, however, for the error terms relating to joint anatomical constraint axis fluctuation, residual force and residual moment. The contribution from the segment length fluctuation term was most sensitive, as a percentage of the GRF, to the choice of cut-off frequency, increasing to 6.7 % and 11.0% for the vertical and anterior/posterior components, respectively, at a cut-off frequency of 50 Hz.

****Table 1 near here****

Discussion

To the best of the authors' knowledge, this study is the first to propose a method for detailed estimation of the influence of modelling errors on derived contributions to variables such as the ground reaction force. The sources of error considered here included body segment parameter errors, geometric measurement errors caused by the fluctuation in position of markers attached to body segments arising from skin motion artefacts, and modelling errors mainly due to segments' elastic deformation. The method has been shown to be effective in determining the contributions to the ground reaction forces from both individual joint torques and a number of sources of modelling error: the new model generated contributions from the named model and error terms whose sum was equal to the measured ground reaction force. By contrast, it is difficult for conventional methods, which utilise Kane's method or the Newton-Euler method, to derive dynamics equations for the ground reaction force because they are unable to take account of fluctuations in segment length or anatomical constraint angles.

The largest error contributions to the ground reaction force in the present study arose from fluctuations in segment length (Figures 5a and 7a) especially at the support leg ankle joint and the virtual joint at ground (Figure 8). However, the magnitudes of these error

contributions were very small relative to the total contribution from 20% of the stance phase onwards. The largest errors were, therefore, seen during the initial contact period when soft tissue motion relative to the underlying skeleton and deformation within the foot of multi-bone structures connecting with ligaments might be expected to be greatest. Fluctuations in length of the support leg segments will cause large error contributions to the ground reaction force when joint angles are selected as generalised variables for the derivation of dynamic equations linked to the ground reaction force. This is because large accelerations of the CG of individual segments arise unless constant values are adopted for the segment lengths. By contrast, the method proposed here does not reconstruct CG positions for the individual segments but instead uses nominal values of those CG positions. Thus, the influences of segment length fluctuation remain comparatively small in magnitude (Figure 5a and 7a). Where the influence of segment length fluctuations is large, the associated errors might be reduced by using an approach such as the point cluster technique (Andriacchi et al., 1998), although the attachment of large numbers of markers is time consuming.

Although the ground reaction force is distributed over the contact surface of the foot segment, where the support-leg foot segment touches its environment (i.e. the ground surface), the model used in this paper assumes that the ground reaction force acts at the COP of the foot and that the foot segment connects to the surface via a virtual joint situated between the ground surface and the COP of the foot segment. Despite the fact that the contact points distributed over the surface of the foot do not move in the foot segment coordinate system, except in the case of foot segment deformation, the COP defined as a representative joint centre point moves largely along the longitudinal axis of the foot during the support phase of rear-foot strikers. This motion causes the overestimation of segment length fluctuations due to the rapid movement of the COP that occurs when using the COP as the virtual joint between the foot and ground. Smoothing with a polynomial function during the induced acceleration analysis would be an effective way to avoid overestimating the contribution of the fluctuation of the COP. When using foot pressure sensing devices (Woodburn & Helliwell, 1996; Putti et al., 2007), or instrumented shoe soles equipped with a number of force sensors (Moriyasu et al., 2010), the actual contact points can be defined

from the sensor positions fixed to the foot segment rather than being estimated from the position of the COP. Additionally, the use of three points fixed to the support-leg foot segment, with forces exerted at those points that are calculated so as to satisfy the equilibrium conditions with respect to force and moment at COP, would be an effective way in the future to reduce the error arising from the COP's fluctuation because the points of the virtual joint between the foot and ground would be fixed to the foot segment.

A number of the possible sources of modelling error made only very small contributions to the calculated ground reaction force. For example, the contributions from the residual force and moment applied at the top of head hardly influenced the outcome. Whether the residual force input is applied at the top of head segment, to the upper trunk segment at the neck joint, or to the upper trunk segment at the torso joint, its contribution to the ground reaction force remains negligible. These results show that neither a Residual Reduction Algorithm (Delp et al., 2007) nor any parameter modification (Kuo, 1998) are absolutely necessary, except for the support leg segments, when implementing an induced-acceleration analysis for evaluating ground reaction force in which the residual error inputs are applied at the top of the head segment.

The anatomical constraint axis fluctuation for a given joint was obtained as a time-curve of the inner product of unit vectors set at the neighbouring segments connecting via that joint, and is inputted into the dynamic contribution function regarding GRF after second-order time differential calculation. Although this value is considered as one of modelling error factors, the error due to this fluctuation is not in the category of cause-effect relationship in an induced-acceleration analysis. Rather the contribution of the "anatomical constraint axes fluctuation" term is similar to an angular acceleration driven system for inducing GRF.

The quantification of modelling error distribution without modification of the measured motion (as done by Delp et al., 2007), and without implementation of dynamic simulation (Kepple et al., 1997; Delp et al., 2007), is useful for clarifying the limitations of modelling the human body as linked rigid segments with nominal values for the body segment parameters, and should be implemented to evaluate the accuracy of the modelling process. The proposed

approach is also beneficial when checking the accuracy of the derivation of the equations of motion for a complex system consisting of a number of segments, such as the whole body, because Equations 7, 15, 16 and 17 can be checked independently and coupling them generates individual contributions whose sum should equal the measured GRF values.

This study has demonstrated that where GRF is chosen as the outcome variable, the contributions from the modelling error are typically small relative to the component associated with joint torques. During the period when they are not negligible, approximately corresponding to initial contact, the current analysis approach allows the origins of those errors to be identified. Modelling errors may be greater where other kinds of variables, such as the joint forces at neck and torso joints, are selected for evaluation because these joints are close to the top of the head where the residual force is being applied. It is, therefore, necessary to check the influences of the modelling error terms in each individual case. Investigation of other types of parameter, such as joint forces, joint constraint moments, whole-body angular momentum with respect to particular axes, and translational and angular velocities of specified segments will also be needed in order to better understand the mechanisms of sporting movements.

Conclusions

A method for estimating modelling error during an induced-acceleration analysis has been introduced, in which the influences of segment length fluctuations, anatomical constraint axes fluctuations, and errors in body segment parameters on the ground reaction forces have been quantified. The practical application of this approach has been demonstrated through the calculation of the contributions of these modelling error terms, alongside the joint torque term, gravitational term, and motion-dependent term, to the ground reaction forces during constant speed running. The joint torque term was the largest contributor to the vertical and anterior/posterior components of ground reaction force; modelling error contributions to both forces were not negligible during the first 20% of the stance phase but their magnitudes and origins could be determined. The results indicate that the proposed method is valid for accurate

quantification of the functional roles of joint torques during running, with only small or identifiable errors arising from the modelling process even when nominal rather than directly-measured values for body segment parameters are used. Further investigation of this type will be needed to determine the magnitude and nature of the modelling error if induced-acceleration methods are applied to quantify the contributions from sources such as joint torques to other biomechanical quantities such as joint forces, joint constraint moments, whole-body angular momentum with respect to particular axes, and translational and angular velocities of individual segments.

References

Anderson, F. C., & Pandy, M. G. (2003). Individual muscle contributions to support in normal walking. *Gait and Posture*, *17*(2), 159-169.

Andriacchi, T. P., Alexander, E. J., Toney, M. K., Dyrby, C., & Sum, J. (1998). A point cluster method for in vivo motion analysis: applied to a study of knee kinematics. *Journal of Biomechanical Engineering*, *120*(6), 743-749.

Delp, S. L., Anderson, F. C., Arnold, A. S., Loan, P., Habib, A., John, C. T., & Thelen, D. G. (2007). OpenSim: open-source software to create and analyze dynamic simulations of movement. *IEEE Transactions on Biomedical Engineering*, *54*(11), 1940-1950.

Fregly, B.J., & Zajac, F.E. (1996). A state-space analysis of mechanical energy generation, absorption, and transfer during pedaling. *Journal of Biomechanics, 29*(1), 81-90.

Fujii, N., & Hubbard, M. (2002). Validation of a three-dimensional baseball pitching model. *Journal of Applied Biomechanics*, *18*(2), 135-154.

Gruber, K., Ruder, H., Denoth, J., & Schneider, K. (1998). A comparative study of impact dynamics: wobbling mass model versus rigid body models. *Journal of Biomechanics, 31*(5), 439-444.

Hamner, S. R., & Delp, S. L. (2013). Muscle contributions to fore-aft and vertical body mass center accelerations over a range of running speeds. *Journal of Biomechanics*, *46*(10), 780-787.

Hamner, S. R., Seth, A., & Delp, S. L. (2010). Muscle contribution to propulsion and support during running. *Journal of Biomechanics, 43*(14), 2709-2716.

Hirashima, M., Yamane, K., Nakamura, Y., & Ohtsuki, T. (2008). Kinetic chain of overarm throwing in terms of joint rotations revealed by induced acceleration analysis. *Journal of Biomechanics, 41*(13), 2874-2883.

Kane, T. R., & Levinson D. A. (1985). *Dynamics: Theory and Applications*. McGraw-Hill, New York, USA.

Kepple, T.M., Siegel, T.L., & Stanhope, S.J. (1997). Relative contributions of the lower extremity joint moments to forward progression and support during stance. *Gait and Posture, 6*, 1-8.

Koike, S., Mori, H., & Ae, M. (2007). Three-dimensional analysis of jump motion based on multi-body dynamics – The contribution of joint torque of the lower limbs to the velocity of the whole-body center of gravity. In F.K. Fuss, A. Subic & S. Ujihashi (Eds.), *The Impact of Technology on Sport II*, CRC Press, Boca Raton, USA, 649-654.

Kuo, A.D. (1998). A least-squares estimation approach to improving the precision of inverse dynamics computations. *Journal of Biomechanical Engineering, 120*(1), 148–159.

Moriyasu, K., Nishiwaki, T., Yamaguchi, T., & Hokkirigawa, K. (2010). New technique of three directional ground reaction force distributions. *Footwear Science, 2*(2), 57–64.

Naito, K., & Maruyama, T. (2008). Contributions of the muscular torques and motion-dependent torques to generate rapid elbow extension during overhand baseball pitching. *Sports Engineering, 11*(1), 47-56.

Neptune, R. R., Kautz, S. A., & Zajac, F. E. (2001). Contributions of the individual ankle plantar flexors to support, forward progression and swing initiation during walking. *Journal of Biomechanics, 34*(11), 1387-1398

Putnam, C.A. (1991). A segment interaction analysis of proximal-to-distal sequential segment motion patterns. *Medicine and Sciences in Sports and Exercise, 23*(1), 130-144.

Putnam, C.A. (1993). Sequential motions of body segments in striking and throwing skills:

Descriptions and explanations. *Journal of Biomechanics*, *26*(1), 125-135.

Putti, A. B., Arnold, G. P., Cochrane, L., & Abboud, R. J. (2007). The Pedar® in-shoe system: Repeatability and normal pressure values. *Gait & Posture*, *25*(3), 401-405.

Sasaki, K., & Neptune, R. R. (2006). Differences in muscle function during walking and running at the same speed. *Journal of Biomechanics*, *39*(11), 2005-2013.

Suzuki, Y., Ae, M., Takenaka, S., & Fujii, N. (2014). Comparison of support leg kinetics between side-step and cross-step cutting techniques. *Sports Biomechanics*, *13*(2), 144-153.

Wells, R.P., & Winter, D.A. (1980). Assessment of signal and noise in the kinematics of normal, pathological and sporting gaits. In *Human Locomotion, I: Pathological gait to the elite athlete* (pp. 92–93). London, Ontario: Canadian Society of Biomechanics.

Woodburn, J., & Helliwell, P. S. (1996). Observations on the F-Scan in-shoe pressure measuring system. *Clinical Biomechanics*, *11*(5), 301-304.

Zajac, F.E., Neptune, R.R., & Kautz, S.A. (2002). Biomechanics and muscle coordination of human walking. Part I: introduction to concepts, power, transfer, dynamics and simulations. *Gait and Posture*, *16*, 215-232.

Zajac, F.E., Neptune, R.R., & Kautz, S.A. (2003). Biomechanics and muscle coordination of human walking. Part II: lessons from dynamical simulations and clinical applications. *Gait and Posture*, *17*, 1-17.

Appendices

Appendix 1

Details of the matrices identified in the dynamical equations in Equation (7) are as follows. Matrices $\boldsymbol{O}$ and $\boldsymbol{E}$, without a subscript, denote the zero and unit matrices with three rows and three columns, and the matrix $\boldsymbol{O}$ with a subscript mxn denotes the zero matrix with m rows and n columns.

$$\boldsymbol{M}\dot{\boldsymbol{V}} = \boldsymbol{P}\boldsymbol{F} + \boldsymbol{Q}\boldsymbol{N} + \boldsymbol{P}_r \boldsymbol{f}_r + \boldsymbol{Q}_r \boldsymbol{n}_r + \boldsymbol{H} + \boldsymbol{G}$$

$$\boldsymbol{V} = \begin{bmatrix} \boldsymbol{V}_1^{\mathrm{T}} & \boldsymbol{V}_2^{\mathrm{T}} & \boldsymbol{V}_3^{\mathrm{T}} & \boldsymbol{V}_4^{\mathrm{T}} & \boldsymbol{V}_5^{\mathrm{T}} \end{bmatrix}^{\mathrm{T}}, \quad \boldsymbol{F} = \begin{bmatrix} \boldsymbol{F}_1^{\mathrm{T}} & \boldsymbol{F}_2^{\mathrm{T}} & \boldsymbol{F}_3^{\mathrm{T}} & \boldsymbol{F}_4^{\mathrm{T}} & \boldsymbol{F}_5^{\mathrm{T}} \end{bmatrix}^{\mathrm{T}}, \quad \boldsymbol{N} = \begin{bmatrix} \boldsymbol{N}_1^{\mathrm{T}} & \boldsymbol{N}_2^{\mathrm{T}} & \boldsymbol{N}_3^{\mathrm{T}} & \boldsymbol{N}_4^{\mathrm{T}} & \boldsymbol{N}_5^{\mathrm{T}} \end{bmatrix}^{\mathrm{T}}$$

$$\boldsymbol{M} = \begin{bmatrix} \boldsymbol{M}_1 & \boldsymbol{O}_{18\times18} & \boldsymbol{O}_{18\times18} & \boldsymbol{O}_{18\times18} & \boldsymbol{O}_{18\times18} \\ \boldsymbol{O}_{18\times18} & \boldsymbol{M}_2 & \boldsymbol{O}_{18\times18} & \boldsymbol{O}_{18\times18} & \boldsymbol{O}_{18\times18} \\ \boldsymbol{O}_{18\times18} & \boldsymbol{O}_{18\times18} & \boldsymbol{M}_3 & \boldsymbol{O}_{18\times18} & \boldsymbol{O}_{18\times18} \\ \boldsymbol{O}_{18\times18} & \boldsymbol{O}_{18\times18} & \boldsymbol{O}_{18\times18} & \boldsymbol{M}_4 & \boldsymbol{O}_{18\times18} \\ \boldsymbol{O}_{18\times18} & \boldsymbol{O}_{18\times18} & \boldsymbol{O}_{18\times18} & \boldsymbol{O}_{18\times18} & \boldsymbol{M}_5 \end{bmatrix}, \quad \boldsymbol{P} = \begin{bmatrix} \boldsymbol{P}_1 & \boldsymbol{O}_{18\times9} & \boldsymbol{O}_{18\times12} & \boldsymbol{O}_{18\times9} & \boldsymbol{O}_{18\times6} \\ \boldsymbol{O}_{18\times9} & \boldsymbol{P}_2 & \boldsymbol{O}_{18\times12} & \boldsymbol{O}_{18\times9} & \boldsymbol{O}_{18\times6} \\ \boldsymbol{O}_{18\times9} & \boldsymbol{O}_{18\times9} & \boldsymbol{P}_3 & \boldsymbol{O}_{18\times9} & \boldsymbol{O}_{18\times6} \\ \boldsymbol{O}_{18\times9} & \boldsymbol{O}_{18\times9} & \boldsymbol{O}_{18\times12} & \boldsymbol{P}_4 & \boldsymbol{O}_{18\times6} \\ \boldsymbol{P}_{5,1} & \boldsymbol{P}_{5,2} & \boldsymbol{P}_{5,3} & \boldsymbol{P}_{5,4} & \boldsymbol{P}_5 \end{bmatrix},$$

$$\boldsymbol{Q} = \begin{bmatrix} \boldsymbol{Q}_1 & \boldsymbol{O}_{18\times9} & \boldsymbol{O}_{18\times12} & \boldsymbol{O}_{18\times9} & \boldsymbol{O}_{18\times6} \\ \boldsymbol{O}_{18\times9} & \boldsymbol{Q}_2 & \boldsymbol{O}_{18\times12} & \boldsymbol{O}_{18\times9} & \boldsymbol{O}_{18\times6} \\ \boldsymbol{O}_{18\times9} & \boldsymbol{O}_{18\times9} & \boldsymbol{Q}_3 & \boldsymbol{O}_{18\times9} & \boldsymbol{O}_{18\times6} \\ \boldsymbol{O}_{18\times9} & \boldsymbol{O}_{18\times9} & \boldsymbol{O}_{18\times12} & \boldsymbol{Q}_4 & \boldsymbol{O}_{18\times6} \\ \boldsymbol{Q}_{5,1} & \boldsymbol{Q}_{5,2} & \boldsymbol{Q}_{5,3} & \boldsymbol{Q}_{5,4} & \boldsymbol{Q}_5 \end{bmatrix}, \boldsymbol{P}_r = \begin{bmatrix} \boldsymbol{O}_{18\times3} \\ \boldsymbol{O}_{18\times3} \\ \boldsymbol{O}_{18\times3} \\ \boldsymbol{O}_{18\times3} \\ \boldsymbol{P}_{r,5} \end{bmatrix}, \quad \boldsymbol{Q}_r = \begin{bmatrix} \boldsymbol{O}_{18\times3} \\ \boldsymbol{O}_{18\times3} \\ \boldsymbol{O}_{18\times3} \\ \boldsymbol{O}_{18\times3} \\ \boldsymbol{Q}_{r,5} \end{bmatrix}, \quad \boldsymbol{H} = \begin{bmatrix} \boldsymbol{H}_1 \\ \boldsymbol{H}_2 \\ \boldsymbol{H}_3 \\ \boldsymbol{H}_4 \\ \boldsymbol{H}_5 \end{bmatrix}, \quad \boldsymbol{G} = \begin{bmatrix} \boldsymbol{G}_1 \\ \boldsymbol{G}_2 \\ \boldsymbol{G}_3 \\ \boldsymbol{G}_4 \\ \boldsymbol{G}_5 \end{bmatrix}$$

$$\boldsymbol{V}_k = \begin{bmatrix} \dot{\boldsymbol{x}}_{k,1}^{\mathrm{T}} & \boldsymbol{\omega}_{k,1}^{\mathrm{T}} & \dot{\boldsymbol{x}}_{k,2}^{\mathrm{T}} & \boldsymbol{\omega}_{k,2}^{\mathrm{T}} & \dot{\boldsymbol{x}}_{k,3}^{\mathrm{T}} & \boldsymbol{\omega}_{k,3}^{\mathrm{T}} \end{bmatrix}^{\mathrm{T}} \quad (k = 1,\ 2, \cdots,\ 5)$$

$$\boldsymbol{F}_k = \begin{bmatrix} \boldsymbol{f}_{k,1}^{\mathrm{T}} & \boldsymbol{f}_{k,2}^{\mathrm{T}} & \boldsymbol{f}_{k,3}^{\mathrm{T}} \end{bmatrix}^{\mathrm{T}} \quad (k = 1,\ 2,\ 4), \qquad \boldsymbol{F}_k = \begin{bmatrix} \boldsymbol{f}_{k,1}^{\mathrm{T}} & \boldsymbol{f}_{k,2}^{\mathrm{T}} \end{bmatrix}^{\mathrm{T}} \quad (k = 5)$$

$$\boldsymbol{F}_k = \begin{bmatrix} \boldsymbol{f}_{k,1}^{\mathrm{T}} & \boldsymbol{f}_{k,2}^{\mathrm{T}} & \boldsymbol{f}_{k,3}^{\mathrm{T}} & -\boldsymbol{f}_{\mathrm{GRF}}^{\mathrm{T}} \end{bmatrix}^{\mathrm{T}} \quad (k = 3)$$

$$\boldsymbol{N}_k = \begin{bmatrix} \boldsymbol{n}_{k,1}^{\mathrm{T}} & \boldsymbol{n}_{k,2}^{\mathrm{T}} & \boldsymbol{n}_{k,3}^{\mathrm{T}} \end{bmatrix}^{\mathrm{T}} \quad (k = 1,\ 2,\ 4,\ 5)$$

$$\boldsymbol{n}_k = \begin{bmatrix} \boldsymbol{n}_{k,1}^{\mathrm{T}} & \boldsymbol{n}_{k,2}^{\mathrm{T}} & \boldsymbol{n}_{k,3}^{\mathrm{T}} & -\boldsymbol{n}_{\mathrm{GRF}}^{\mathrm{T}} \end{bmatrix}^{\mathrm{T}} \quad (k = 3)$$

$$\boldsymbol{M}_k = \mathrm{block\ diag}\left\{ m_{k,1}\boldsymbol{E} \quad \hat{\boldsymbol{I}}_{k,1} \quad m_{k,2}\boldsymbol{E} \quad \hat{\boldsymbol{I}}_{k,2} \quad m_{k,3}\boldsymbol{E} \quad \hat{\boldsymbol{I}}_{k,3} \right\}$$

$$\boldsymbol{P}_k = \begin{bmatrix} \boldsymbol{E} & -\boldsymbol{E} & \boldsymbol{O} \\ \left[\boldsymbol{r}_{k,1,\overline{\mathrm{cg\text{-}P}}} \times \right] & -\left[\boldsymbol{r}_{k,1,\overline{\mathrm{cg\text{-}D}}} \times \right] & \boldsymbol{O} \\ \boldsymbol{O} & \boldsymbol{E} & -\boldsymbol{E} \\ \boldsymbol{O} & \left[\boldsymbol{r}_{k,2,\overline{\mathrm{cg\text{-}P}}} \times \right] & -\left[\boldsymbol{r}_{k,2,\overline{\mathrm{cg\text{-}D}}} \times \right] \\ \boldsymbol{O} & \boldsymbol{O} & \boldsymbol{E} \\ \boldsymbol{O} & \boldsymbol{O} & \left[\boldsymbol{r}_{k,3,\overline{\mathrm{cg\text{-}P}}} \times \right] \end{bmatrix} \quad (k = 1,\ 2,\ 4,\ 5)$$

$$\boldsymbol{P}_k = \begin{bmatrix} \boldsymbol{E} & -\boldsymbol{E} & \boldsymbol{O} & \boldsymbol{O} \\ \left[\boldsymbol{r}_{k,1,\overline{\text{cg-P}}}\times\right] & -\left[\boldsymbol{r}_{k,1,\overline{\text{cg-D}}}\times\right] & \boldsymbol{O} & \boldsymbol{O} \\ \boldsymbol{O} & \boldsymbol{E} & -\boldsymbol{E} & \boldsymbol{O} \\ \boldsymbol{O} & \left[\boldsymbol{r}_{k,2,\overline{\text{cg-P}}}\times\right] & -\left[\boldsymbol{r}_{k,2,\overline{\text{cg-D}}}\times\right] & \boldsymbol{O} \\ \boldsymbol{O} & \boldsymbol{O} & \boldsymbol{E} & -\boldsymbol{E} \\ \boldsymbol{O} & \boldsymbol{O} & \left[\boldsymbol{r}_{k,3,\overline{\text{cg-P}}}\times\right] & -\left[\boldsymbol{r}_{k,3,\overline{\text{cg-COP}}}\times\right] \end{bmatrix} \quad (k=3)$$

$$\boldsymbol{P}_{5,1} = \begin{bmatrix} \boldsymbol{O} & \boldsymbol{O} & \boldsymbol{O} \\ \boldsymbol{O} & \boldsymbol{O} & \boldsymbol{O} \\ -\boldsymbol{E} & \boldsymbol{O} & \boldsymbol{O} \\ -\left[\boldsymbol{r}_{5,2,\overline{\text{cg-DR}}}\times\right] & \boldsymbol{O} & \boldsymbol{O} \\ \boldsymbol{O} & \boldsymbol{O} & \boldsymbol{O} \\ \boldsymbol{O} & \boldsymbol{O} & \boldsymbol{O} \\ \boldsymbol{O} & \boldsymbol{O} & \boldsymbol{O} \end{bmatrix}, \boldsymbol{P}_{5,2} = \begin{bmatrix} \boldsymbol{O} & \boldsymbol{O} & \boldsymbol{O} \\ \boldsymbol{O} & \boldsymbol{O} & \boldsymbol{O} \\ -\boldsymbol{E} & \boldsymbol{O} & \boldsymbol{O} \\ -\left[\boldsymbol{r}_{5,2,\overline{\text{cg-DL}}}\times\right] & \boldsymbol{O} & \boldsymbol{O} \\ \boldsymbol{O} & \boldsymbol{O} & \boldsymbol{O} \\ \boldsymbol{O} & \boldsymbol{O} & \boldsymbol{O} \\ \boldsymbol{O} & \boldsymbol{O} & \boldsymbol{O} \end{bmatrix}, \boldsymbol{P}_{5,3} = \begin{bmatrix} \boldsymbol{O} & \boldsymbol{O} & \boldsymbol{O} \\ \boldsymbol{O} & \boldsymbol{O} & \boldsymbol{O} \\ \boldsymbol{O} & \boldsymbol{O} & \boldsymbol{O} \\ \boldsymbol{O} & \boldsymbol{O} & \boldsymbol{O} \\ -\boldsymbol{E} & \boldsymbol{O} & \boldsymbol{O} \\ -\left[\boldsymbol{r}_{5,3,\overline{\text{cg-DR}}}\times\right] & \boldsymbol{O} & \boldsymbol{O} \\ \boldsymbol{O} & \boldsymbol{O} & \boldsymbol{O} \end{bmatrix},$$

$$\boldsymbol{P}_{5,4} = \begin{bmatrix} \boldsymbol{O} & \boldsymbol{O} & \boldsymbol{O} \\ \boldsymbol{O} & \boldsymbol{O} & \boldsymbol{O} \\ \boldsymbol{O} & \boldsymbol{O} & \boldsymbol{O} \\ \boldsymbol{O} & \boldsymbol{O} & \boldsymbol{O} \\ -\boldsymbol{E} & \boldsymbol{O} & \boldsymbol{O} \\ -\left[\boldsymbol{r}_{5,3,\overline{\text{cg-DL}}}\times\right] & \boldsymbol{O} & \boldsymbol{O} \\ \boldsymbol{O} & \boldsymbol{O} & \boldsymbol{O} \end{bmatrix}$$

$$\boldsymbol{Q}_k = \begin{bmatrix} \boldsymbol{O} & \boldsymbol{O} & \boldsymbol{O} \\ \boldsymbol{E} & -\boldsymbol{E} & \boldsymbol{O} \\ \boldsymbol{O} & \boldsymbol{O} & \boldsymbol{O} \\ \boldsymbol{O} & \boldsymbol{E} & -\boldsymbol{E} \\ \boldsymbol{O} & \boldsymbol{O} & \boldsymbol{O} \\ \boldsymbol{O} & \boldsymbol{O} & \boldsymbol{E} \end{bmatrix} \quad (k=1,\ 2,\ 4,\ 5)$$

$$\boldsymbol{Q}_k = \begin{bmatrix} \boldsymbol{O} & \boldsymbol{O} & \boldsymbol{O} & \boldsymbol{O} \\ \boldsymbol{E} & -\boldsymbol{E} & \boldsymbol{O} & \boldsymbol{O} \\ \boldsymbol{O} & \boldsymbol{O} & \boldsymbol{O} & \boldsymbol{O} \\ \boldsymbol{O} & \boldsymbol{E} & -\boldsymbol{E} & \boldsymbol{O} \\ \boldsymbol{O} & \boldsymbol{O} & \boldsymbol{O} & \boldsymbol{O} \\ \boldsymbol{O} & \boldsymbol{O} & \boldsymbol{E} & -\boldsymbol{E} \end{bmatrix} \quad (k=3)$$

$$\boldsymbol{Q}_{5,1} = \begin{bmatrix} \boldsymbol{O} & \boldsymbol{O} & \boldsymbol{O} \\ \boldsymbol{O} & \boldsymbol{O} & \boldsymbol{O} \\ \boldsymbol{O} & \boldsymbol{O} & \boldsymbol{O} \\ -\boldsymbol{E} & \boldsymbol{O} & \boldsymbol{O} \\ \boldsymbol{O} & \boldsymbol{O} & \boldsymbol{O} \\ \boldsymbol{O} & \boldsymbol{O} & \boldsymbol{O} \\ \boldsymbol{O} & \boldsymbol{O} & \boldsymbol{O} \end{bmatrix}, \boldsymbol{Q}_{5,2} = \begin{bmatrix} \boldsymbol{O} & \boldsymbol{O} & \boldsymbol{O} \\ \boldsymbol{O} & \boldsymbol{O} & \boldsymbol{O} \\ \boldsymbol{O} & \boldsymbol{O} & \boldsymbol{O} \\ -\boldsymbol{E} & \boldsymbol{O} & \boldsymbol{O} \\ \boldsymbol{O} & \boldsymbol{O} & \boldsymbol{O} \\ \boldsymbol{O} & \boldsymbol{O} & \boldsymbol{O} \\ \boldsymbol{O} & \boldsymbol{O} & \boldsymbol{O} \end{bmatrix}, \boldsymbol{Q}_{5,3} = \begin{bmatrix} \boldsymbol{O} & \boldsymbol{O} & \boldsymbol{O} \\ \boldsymbol{O} & \boldsymbol{O} & \boldsymbol{O} \\ \boldsymbol{O} & \boldsymbol{O} & \boldsymbol{O} \\ \boldsymbol{O} & \boldsymbol{O} & \boldsymbol{O} \\ \boldsymbol{O} & \boldsymbol{O} & \boldsymbol{O} \\ -\boldsymbol{E} & \boldsymbol{O} & \boldsymbol{O} \\ \boldsymbol{O} & \boldsymbol{O} & \boldsymbol{O} \end{bmatrix}, \boldsymbol{Q}_{5,4} = \begin{bmatrix} \boldsymbol{O} & \boldsymbol{O} & \boldsymbol{O} \\ \boldsymbol{O} & \boldsymbol{O} & \boldsymbol{O} \\ \boldsymbol{O} & \boldsymbol{O} & \boldsymbol{O} \\ \boldsymbol{O} & \boldsymbol{O} & \boldsymbol{O} \\ \boldsymbol{O} & \boldsymbol{O} & \boldsymbol{O} \\ -\boldsymbol{E} & \boldsymbol{O} & \boldsymbol{O} \\ \boldsymbol{O} & \boldsymbol{O} & \boldsymbol{O} \end{bmatrix}$$

$$\boldsymbol{P}_{\mathrm{r},5}=\begin{bmatrix} \boldsymbol{E} & -\boldsymbol{E} & \boldsymbol{O} \\ \left[\boldsymbol{r}_{5,1,\overline{\mathrm{cg\text{-}P}}}\times\right] & -\left[\boldsymbol{r}_{5,1,\overline{\mathrm{cg\text{-}D}}}\times\right] & \boldsymbol{O} \\ \boldsymbol{O} & \boldsymbol{E} & -\boldsymbol{E} \\ \boldsymbol{O} & \left[\boldsymbol{r}_{5,2,\overline{\mathrm{cg\text{-}P}}}\times\right] & -\left[\boldsymbol{r}_{5,2,\overline{\mathrm{cg\text{-}D}}}\times\right] \\ \boldsymbol{O} & \boldsymbol{O} & \boldsymbol{E} \\ \boldsymbol{O} & \boldsymbol{O} & \left[\boldsymbol{r}_{5,3,\overline{\mathrm{cg\text{-}P}}}\times\right] \end{bmatrix}$$

$$\boldsymbol{Q}_{\mathrm{r},5}=\begin{bmatrix} \boldsymbol{O} & \boldsymbol{O} & \boldsymbol{O} \\ \boldsymbol{E} & -\boldsymbol{E} & \boldsymbol{O} \\ \boldsymbol{O} & \boldsymbol{O} & \boldsymbol{O} \\ \boldsymbol{O} & \boldsymbol{E} & -\boldsymbol{E} \\ \boldsymbol{O} & \boldsymbol{O} & \boldsymbol{O} \\ \boldsymbol{O} & \boldsymbol{O} & \boldsymbol{E} \end{bmatrix}$$

$$\boldsymbol{G}_k=\begin{bmatrix} m_{k,1}\boldsymbol{g} \\ \boldsymbol{O}_{3\times1} \\ m_{k,2}\boldsymbol{g} \\ \boldsymbol{O}_{3\times1} \\ m_{k,3}\boldsymbol{g} \\ \boldsymbol{O}_{3\times1} \end{bmatrix},\ \boldsymbol{H}_k=\begin{bmatrix} \boldsymbol{O}_{3\times1} \\ -\boldsymbol{\omega}_{k,1}\times(\hat{\boldsymbol{I}}_{k,1}\boldsymbol{\omega}_{k,1}) \\ \boldsymbol{O}_{3\times1} \\ -\boldsymbol{\omega}_{k,2}\times(\hat{\boldsymbol{I}}_{k,2}\boldsymbol{\omega}_{k,2}) \\ \boldsymbol{O}_{3\times1} \\ -\boldsymbol{\omega}_{k,3}\times(\hat{\boldsymbol{I}}_{k,3}\boldsymbol{\omega}_{k,3}) \end{bmatrix}$$

Appendix 2

Details of the matrices identified in the constraint equations in Equation (11) are as follows:

$$\boldsymbol{CV} = \dot{\boldsymbol{\eta}}$$

$$\boldsymbol{C} = \begin{bmatrix} \boldsymbol{C}_1 & \boldsymbol{O}_{9\times18} & \boldsymbol{O}_{9\times18} & \boldsymbol{O}_{9\times18} & \boldsymbol{C}_{1,5} \\ \boldsymbol{O}_{9\times18} & \boldsymbol{C}_2 & \boldsymbol{O}_{9\times18} & \boldsymbol{O}_{9\times18} & \boldsymbol{C}_{2,5} \\ \boldsymbol{O}_{12\times18} & \boldsymbol{O}_{12\times18} & \boldsymbol{C}_3 & \boldsymbol{O}_{12\times18} & \boldsymbol{C}_{3,5} \\ \boldsymbol{O}_{9\times18} & \boldsymbol{O}_{9\times18} & \boldsymbol{O}_{9\times18} & \boldsymbol{C}_4 & \boldsymbol{C}_{4,5} \\ \boldsymbol{O}_{6\times18} & \boldsymbol{O}_{6\times18} & \boldsymbol{O}_{6\times18} & \boldsymbol{O}_{6\times18} & \boldsymbol{C}_5 \end{bmatrix}, \quad \boldsymbol{\eta} = \begin{bmatrix} \boldsymbol{\eta}_1 \\ \boldsymbol{\eta}_2 \\ \boldsymbol{\eta}_3 \\ \boldsymbol{\eta}_4 \\ \boldsymbol{\eta}_5 \end{bmatrix}$$

$$\boldsymbol{C}_k = \begin{bmatrix} -\boldsymbol{E} & \left[\boldsymbol{r}_{k,1,\overline{\text{cg-P}}}\times\right] & \boldsymbol{O} & \boldsymbol{O} & \boldsymbol{O} & \boldsymbol{O} \\ \boldsymbol{E} & -\left[\boldsymbol{r}_{k,1,\overline{\text{cg-D}}}\times\right] & -\boldsymbol{E} & \left[\boldsymbol{r}_{k,2,\overline{\text{cg-P}}}\times\right] & \boldsymbol{O} & \boldsymbol{O} \\ \boldsymbol{O} & \boldsymbol{O} & \boldsymbol{E} & -\left[\boldsymbol{r}_{k,2,\overline{\text{cg-D}}}\times\right] & -\boldsymbol{E} & \left[\boldsymbol{r}_{k,3,\overline{\text{cg-P}}}\times\right] \end{bmatrix} \left(k = 1,\ 2,\ 4,\ 5\right)$$

$$\boldsymbol{C}_k = \begin{bmatrix} -\boldsymbol{E} & \left[\boldsymbol{r}_{k,1,\overline{\text{cg-P}}}\times\right] & \boldsymbol{O} & \boldsymbol{O} & \boldsymbol{O} & \boldsymbol{O} \\ \boldsymbol{E} & -\left[\boldsymbol{r}_{k,1,\overline{\text{cg-D}}}\times\right] & -\boldsymbol{E} & \left[\boldsymbol{r}_{k,2,\overline{\text{cg-P}}}\times\right] & \boldsymbol{O} & \boldsymbol{O} \\ \boldsymbol{O} & \boldsymbol{O} & \boldsymbol{E} & -\left[\boldsymbol{r}_{k,2,\overline{\text{cg-D}}}\times\right] & -\boldsymbol{E} & \left[\boldsymbol{r}_{k,3,\overline{\text{cg-P}}}\times\right] \\ \boldsymbol{O} & \boldsymbol{O} & \boldsymbol{O} & \boldsymbol{O} & \boldsymbol{E} & -\left[\boldsymbol{r}_{k,2,\overline{\text{cg-COP}}}\times\right] \end{bmatrix} \left(k = 3\right)$$

Appendix 3

Details of the matrices identified in the anatomical constraint equations in Equation (14) are as follows:

$$\boldsymbol{A}\boldsymbol{V} = \dot{\boldsymbol{\varphi}}$$

$$\boldsymbol{A} = \begin{bmatrix} \boldsymbol{A}_1 & \boldsymbol{O}_{2\times18} & \boldsymbol{O}_{2\times18} & \boldsymbol{O}_{2\times18} & \boldsymbol{O}_{2\times18} \\ \boldsymbol{O}_{2\times18} & \boldsymbol{A}_2 & \boldsymbol{O}_{2\times18} & \boldsymbol{O}_{2\times18} & \boldsymbol{O}_{2\times18} \\ \boldsymbol{O}_{2\times18} & \boldsymbol{O}_{2\times18} & \boldsymbol{A}_3 & \boldsymbol{O}_{2\times18} & \boldsymbol{O}_{2\times18} \\ \boldsymbol{O}_{2\times18} & \boldsymbol{O}_{2\times18} & \boldsymbol{O}_{2\times18} & \boldsymbol{A}_4 & \boldsymbol{O}_{2\times18} \end{bmatrix}, \quad \boldsymbol{\varphi} = \begin{bmatrix} \boldsymbol{\varphi}_1 \\ \boldsymbol{\varphi}_2 \\ \boldsymbol{\varphi}_3 \\ \boldsymbol{\varphi}_4 \end{bmatrix}, \quad \boldsymbol{\varphi}_k = \begin{bmatrix} \boldsymbol{\varphi}_{k,2}(t) \\ \boldsymbol{\varphi}_{k,3}(t) \end{bmatrix} \quad (k=1,2,3,4)$$

$$\boldsymbol{A}_k = \begin{bmatrix} \boldsymbol{O}_{1\times3} & -\boldsymbol{e}_{k,2,z}^{\mathrm{T}}\left[\boldsymbol{e}_{k,1,x}\times\right] & \boldsymbol{O}_{1\times3} & -\boldsymbol{e}_{k,1,x}^{\mathrm{T}}\left[\boldsymbol{e}_{k,2,z}\times\right] & \boldsymbol{O}_{1\times3} & \boldsymbol{O}_{1\times3} \\ \boldsymbol{O}_{1\times3} & \boldsymbol{O}_{1\times3} & \boldsymbol{O}_{1\times3} & -\boldsymbol{e}_{k,3,y}^{\mathrm{T}}\left[\boldsymbol{e}_{k,2,x}\times\right] & \boldsymbol{O}_{1\times3} & -\boldsymbol{e}_{k,2,x}^{\mathrm{T}}\left[\boldsymbol{e}_{k,3,y}\times\right] \end{bmatrix} \quad (k=1,\ 2)$$

$$\boldsymbol{A}_k = \begin{bmatrix} \boldsymbol{O}_{1\times3} & -\boldsymbol{e}_{k,2,z}^{\mathrm{T}}\left[\boldsymbol{e}_{k,1,x}\times\right] & \boldsymbol{O}_{1\times3} & -\boldsymbol{e}_{k,1,x}^{\mathrm{T}}\left[\boldsymbol{e}_{k,2,z}\times\right] & \boldsymbol{O}_{1\times3} & \boldsymbol{O}_{1\times3} \\ \boldsymbol{O}_{1\times3} & \boldsymbol{O}_{1\times3} & \boldsymbol{O}_{1\times3} & -\boldsymbol{e}_{k,3,z}^{\mathrm{T}}\left[\boldsymbol{e}_{k,2,x}\times\right] & \boldsymbol{O}_{1\times3} & -\boldsymbol{e}_{k,2,x}^{\mathrm{T}}\left[\boldsymbol{e}_{k,3,z}\times\right] \end{bmatrix} \quad (k=3,\ 4)$$

Appendix 4

Details of the matrices identified in Equation (15) are as follows:

$$\boldsymbol{N} = \boldsymbol{S}_{\mathrm{a}}\boldsymbol{T}_{\mathrm{a}} + \boldsymbol{S}_{\mathrm{p}}\boldsymbol{T}_{\mathrm{p}}$$

$$\boldsymbol{S}_{\mathrm{a}} = \begin{bmatrix} \boldsymbol{S}_{\mathrm{a},1} & \boldsymbol{O}_{9\times7} & \boldsymbol{O}_{9\times10} & \boldsymbol{O}_{9\times7} & \boldsymbol{O}_{9\times6} \\ \boldsymbol{O}_{9\times7} & \boldsymbol{S}_{\mathrm{a},2} & \boldsymbol{O}_{9\times10} & \boldsymbol{O}_{9\times7} & \boldsymbol{O}_{9\times6} \\ \boldsymbol{O}_{12\times7} & \boldsymbol{O}_{12\times7} & \boldsymbol{S}_{\mathrm{a},3} & \boldsymbol{O}_{12\times7} & \boldsymbol{O}_{12\times6} \\ \boldsymbol{O}_{9\times7} & \boldsymbol{O}_{9\times7} & \boldsymbol{O}_{9\times10} & \boldsymbol{S}_{\mathrm{a},4} & \boldsymbol{O}_{9\times6} \\ \boldsymbol{O}_{6\times7} & \boldsymbol{O}_{6\times7} & \boldsymbol{O}_{6\times10} & \boldsymbol{O}_{6\times7} & \boldsymbol{S}_{\mathrm{a},5} \end{bmatrix}, \quad \boldsymbol{S}_{\mathrm{p}} = \begin{bmatrix} \boldsymbol{S}_{\mathrm{p},1} & \boldsymbol{O}_{9\times2} & \boldsymbol{O}_{9\times2} & \boldsymbol{O}_{9\times2} \\ \boldsymbol{O}_{9\times2} & \boldsymbol{S}_{\mathrm{p},2} & \boldsymbol{O}_{9\times2} & \boldsymbol{O}_{9\times2} \\ \boldsymbol{O}_{12\times2} & \boldsymbol{O}_{12\times2} & \boldsymbol{S}_{\mathrm{p},3} & \boldsymbol{O}_{12\times2} \\ \boldsymbol{O}_{9\times2} & \boldsymbol{O}_{9\times2} & \boldsymbol{O}_{9\times2} & \boldsymbol{S}_{\mathrm{p},4} \\ \boldsymbol{O}_{6\times2} & \boldsymbol{O}_{6\times2} & \boldsymbol{O}_{6\times2} & \boldsymbol{O}_{6\times2} \end{bmatrix}, \quad \boldsymbol{T}_{\mathrm{a}} = \begin{bmatrix} \boldsymbol{T}_{\mathrm{a},1} \\ \boldsymbol{T}_{\mathrm{a},2} \\ \boldsymbol{T}_{\mathrm{a},3} \\ \boldsymbol{T}_{\mathrm{a},4} \\ \boldsymbol{T}_{\mathrm{a},5} \end{bmatrix}, \quad \boldsymbol{T}_{\mathrm{p}} = \begin{bmatrix} \boldsymbol{T}_{\mathrm{p},1} \\ \boldsymbol{T}_{\mathrm{p},2} \\ \boldsymbol{T}_{\mathrm{p},3} \\ \boldsymbol{T}_{\mathrm{p},4} \\ \boldsymbol{T}_{\mathrm{p},5} \end{bmatrix}$$

$$\boldsymbol{S}_{\mathrm{a},k} = \begin{bmatrix} \boldsymbol{K}_{k,1}^{-1} & \boldsymbol{O}_{3\times2} & \boldsymbol{O}_{3\times2} \\ \boldsymbol{O}_{3\times3} & \boldsymbol{K}_{k,2}^{-1}\begin{bmatrix} 1 & 0 & 0 \\ 0 & 0 & 1 \end{bmatrix}^{\mathrm{T}} & \boldsymbol{O}_{3\times2} \\ \boldsymbol{O}_{3\times3} & \boldsymbol{O}_{3\times2} & \boldsymbol{K}_{k,3}^{-1}\begin{bmatrix} 1 & 0 & 0 \\ 0 & 1 & 0 \end{bmatrix}^{\mathrm{T}} \end{bmatrix} \quad (k = 1, 2)$$

$$\boldsymbol{S}_{\mathrm{a},k} = \begin{bmatrix} \boldsymbol{K}_{k,1}^{-1} & \boldsymbol{O}_{3\times2} & \boldsymbol{O}_{3\times2} & \boldsymbol{O}_{3\times3} \\ \boldsymbol{O}_{3\times3} & \boldsymbol{K}_{k,2}^{-1}\begin{bmatrix} 1 & 0 & 0 \\ 0 & 0 & 1 \end{bmatrix}^{\mathrm{T}} & \boldsymbol{O}_{3\times2} & \boldsymbol{O}_{3\times3} \\ \boldsymbol{O}_{3\times3} & \boldsymbol{O}_{3\times2} & \boldsymbol{K}_{k,3}^{-1}\begin{bmatrix} 1 & 0 & 0 \\ 0 & 0 & 1 \end{bmatrix}^{\mathrm{T}} & \boldsymbol{O}_{3\times3} \\ \boldsymbol{O}_{3\times3} & \boldsymbol{O}_{3\times2} & \boldsymbol{O}_{3\times2} & \boldsymbol{K}_{k,\mathrm{COP}}^{-1} \end{bmatrix} \quad (k = 3), \qquad \boldsymbol{K}_{k,\mathrm{COP}} = \begin{bmatrix} 1 & 0 & 0 \\ 0 & 1 & 0 \\ 0 & 0 & 1 \end{bmatrix}$$

$$\boldsymbol{S}_{\mathrm{a},k} = \begin{bmatrix} \boldsymbol{K}_{k,1}^{-1} & \boldsymbol{O}_{3\times2} & \boldsymbol{O}_{3\times2} \\ \boldsymbol{O}_{3\times3} & \boldsymbol{K}_{k,2}^{-1}\begin{bmatrix} 1 & 0 & 0 \\ 0 & 0 & 1 \end{bmatrix}^{\mathrm{T}} & \boldsymbol{O}_{3\times2} \\ \boldsymbol{O}_{3\times3} & \boldsymbol{O}_{3\times2} & \boldsymbol{K}_{k,3}^{-1}\begin{bmatrix} 1 & 0 & 0 \\ 0 & 0 & 1 \end{bmatrix}^{\mathrm{T}} \end{bmatrix} \quad (k = 4)$$

$$\boldsymbol{S}_{\mathrm{a},k} = \begin{bmatrix} \boldsymbol{K}_{k,1}^{-1} & \boldsymbol{O}_{3\times3} \\ \boldsymbol{O}_{3\times3} & \boldsymbol{K}_{k,2}^{-1} \end{bmatrix} \quad (k = 5)$$

$$\boldsymbol{S}_{\mathrm{p},k} = \begin{bmatrix} \boldsymbol{O}_{3\times1} & \boldsymbol{O}_{3\times1} \\ \boldsymbol{K}_{k,2}^{-1}\begin{bmatrix} 0 & 1 & 0 \end{bmatrix}^{\mathrm{T}} & \boldsymbol{O}_{3\times1} \\ \boldsymbol{O}_{3\times1} & \boldsymbol{K}_{k,3}^{-1}\begin{bmatrix} 0 & 0 & 1 \end{bmatrix}^{\mathrm{T}} \end{bmatrix} \quad (k = 1, 2)$$

$$\boldsymbol{S}_{\mathrm{p},k} = \begin{bmatrix} \boldsymbol{O}_{3\times1} & \boldsymbol{O}_{3\times1} \\ \boldsymbol{K}_{k,2}^{-1}\begin{bmatrix} 0 & 1 & 0 \end{bmatrix}^{\mathrm{T}} & \boldsymbol{O}_{3\times1} \\ \boldsymbol{O}_{3\times1} & \boldsymbol{K}_{k,3}^{-1}\begin{bmatrix} 0 & 1 & 0 \end{bmatrix}^{\mathrm{T}} \\ \boldsymbol{O}_{3\times1} & \boldsymbol{O}_{3\times1} \end{bmatrix} \quad (k = 3)$$

$$\boldsymbol{S}_{\mathrm{p},k} = \begin{bmatrix} \boldsymbol{O}_{3\times1} & \boldsymbol{O}_{3\times1} \\ \boldsymbol{K}_{k,2}^{-1}\begin{bmatrix}0 & 1 & 0\end{bmatrix}^{\mathrm{T}} & \boldsymbol{O}_{3\times1} \\ \boldsymbol{O}_{3\times1} & \boldsymbol{K}_{k,3}^{-1}\begin{bmatrix}0 & 1 & 0\end{bmatrix}^{\mathrm{T}} \end{bmatrix} \quad (k=4)$$

$$\boldsymbol{K}_{k,j} = \begin{bmatrix} \boldsymbol{e}_{k,j,x} & \boldsymbol{e}_{k,j,y} & \boldsymbol{e}_{k,j,z} \end{bmatrix}$$

where the unit vector $\boldsymbol{e}_{k,j,i}$ denotes the i-th axial vector of the j-th joint in the k-th group.

$$\boldsymbol{T}_{\mathrm{p},k} = \begin{bmatrix} \tau_{k,2,\mathrm{y}} & \tau_{k,3,\mathrm{z}} \end{bmatrix}^{\mathrm{T}} \quad (k=1,\ 2)$$

$$\boldsymbol{T}_{\mathrm{p},k} = \begin{bmatrix} \tau_{k,2,\mathrm{y}} & \tau_{k,3,\mathrm{y}} \end{bmatrix}^{\mathrm{T}} \quad (k=3,\ 4)$$

$$\boldsymbol{T}_{\mathrm{a},k} = \begin{bmatrix} \tau_{k,1,\mathrm{x}} & \tau_{k,1,\mathrm{y}} & \tau_{k,1,\mathrm{z}} & \tau_{k,2,\mathrm{x}} & \tau_{k,2,z} & \tau_{k,3,\mathrm{x}} & \tau_{k,2,y} \end{bmatrix}^{\mathrm{T}} \quad (k=1,\ 2)$$

$$\boldsymbol{T}_{\mathrm{a},k} = \begin{bmatrix} \tau_{k,1,\mathrm{x}} & \tau_{k,1,\mathrm{y}} & \tau_{k,1,\mathrm{z}} & \tau_{k,2,\mathrm{x}} & \tau_{k,2,z} & \tau_{k,3,\mathrm{x}} & \tau_{k,2,z} & 0 & 0 & -n_{\mathrm{COP}} \end{bmatrix}^{\mathrm{T}} \quad (k=3)$$

$$\boldsymbol{T}_{\mathrm{a},k} = \begin{bmatrix} \tau_{k,1,\mathrm{x}} & \tau_{k,1,\mathrm{y}} & \tau_{k,1,\mathrm{z}} & \tau_{k,2,\mathrm{x}} & \tau_{k,2,z} & \tau_{k,3,\mathrm{x}} & \tau_{k,2,z} \end{bmatrix}^{\mathrm{T}} \quad (k=4)$$

Appendix 5

Details of the matrices identified in Equation (19) are as follows:

$$\left.\begin{aligned} &\boldsymbol{A}_{F,Ta}=\boldsymbol{\Phi Q}_a\,,\quad \boldsymbol{A}_{F,V}=\boldsymbol{\Phi H}+\bar{\boldsymbol{H}}_{FV}\boldsymbol{V}\,,\quad \boldsymbol{A}_{F,G}=\boldsymbol{\Phi G}\\ &\boldsymbol{A}_{F,fr}=\boldsymbol{\Phi P}_r\boldsymbol{f}_r\,,\quad \boldsymbol{A}_{F,nr}=\boldsymbol{\Phi Q}_r\,,\quad \boldsymbol{A}_{F\eta}=\bar{\boldsymbol{H}}_{F\eta}\,,\quad \boldsymbol{A}_{F\varphi}=\bar{\boldsymbol{H}}_{F\varphi} \end{aligned}\right\}$$

where the temporary matrices $\boldsymbol{\Phi}$, $\boldsymbol{Q}_{\mathrm{a}}$, $\boldsymbol{Q}_{\mathrm{b}}$, $\bar{\boldsymbol{H}}_{FV}$, $\boldsymbol{\Gamma}$, $\bar{\boldsymbol{H}}_{TV}$, $\bar{\boldsymbol{H}}_{F\eta}$, $\bar{\boldsymbol{H}}_{T\eta}$ and $\bar{\boldsymbol{H}}_{F\varphi}$ are shown as follows:

$$\left.\begin{aligned} &\boldsymbol{\Phi}=\left(\boldsymbol{CM}^{-1}\boldsymbol{P}\right)^{-1}\boldsymbol{CM}^{-1}\left\{\boldsymbol{Q}_p\left(\boldsymbol{\Gamma Q}_p\right)^{-1}\boldsymbol{\Gamma}-\boldsymbol{E}\right\},\\ &\boldsymbol{Q}_{\mathrm{a}}=\boldsymbol{QS}_{\mathrm{a}},\\ &\boldsymbol{Q}_{\mathrm{p}}=\boldsymbol{QS}_{\mathrm{p}},\\ &\bar{\boldsymbol{H}}_{FV}=\left(\boldsymbol{CM}^{-1}\boldsymbol{P}\right)^{-1}\left\{\boldsymbol{CM}^{-1}\boldsymbol{Q}_p\left(\boldsymbol{\Gamma Q}_p\right)^{-1}\bar{\boldsymbol{H}}_{TV}-\dot{\boldsymbol{C}}\right\},\\ &\boldsymbol{\Gamma}=\boldsymbol{AM}^{-1}\left\{\boldsymbol{E}-\boldsymbol{P}\left(\boldsymbol{CM}^{-1}\boldsymbol{P}\right)^{-1}\boldsymbol{CM}^{-1}\right\},\\ &\bar{\boldsymbol{H}}_{TV}=\dot{\boldsymbol{A}}-\boldsymbol{AM}^{-1}\boldsymbol{P}\left(\boldsymbol{CM}^{-1}\boldsymbol{P}\right)^{-1}\dot{\boldsymbol{C}},\\ &\bar{\boldsymbol{H}}_{F\eta}=\left(\boldsymbol{CM}^{-1}\boldsymbol{P}\right)^{-1}\left\{\boldsymbol{CM}^{-1}\boldsymbol{Q}_p\left(\boldsymbol{\Gamma Q}_p\right)^{-1}\bar{\boldsymbol{H}}_{T\eta}+\boldsymbol{E}\right\},\\ &\bar{\boldsymbol{H}}_{T\eta}=\boldsymbol{AM}^{-1}\boldsymbol{P}\left(\boldsymbol{CM}^{-1}\boldsymbol{P}\right)^{-1},\\ &\bar{\boldsymbol{H}}_{F\varphi}=\left(\boldsymbol{CM}^{-1}\boldsymbol{P}\right)^{-1}\boldsymbol{CM}^{-1}\boldsymbol{Q}_p\left(\boldsymbol{\Gamma Q}_p\right)^{-1} \end{aligned}\right\}$$

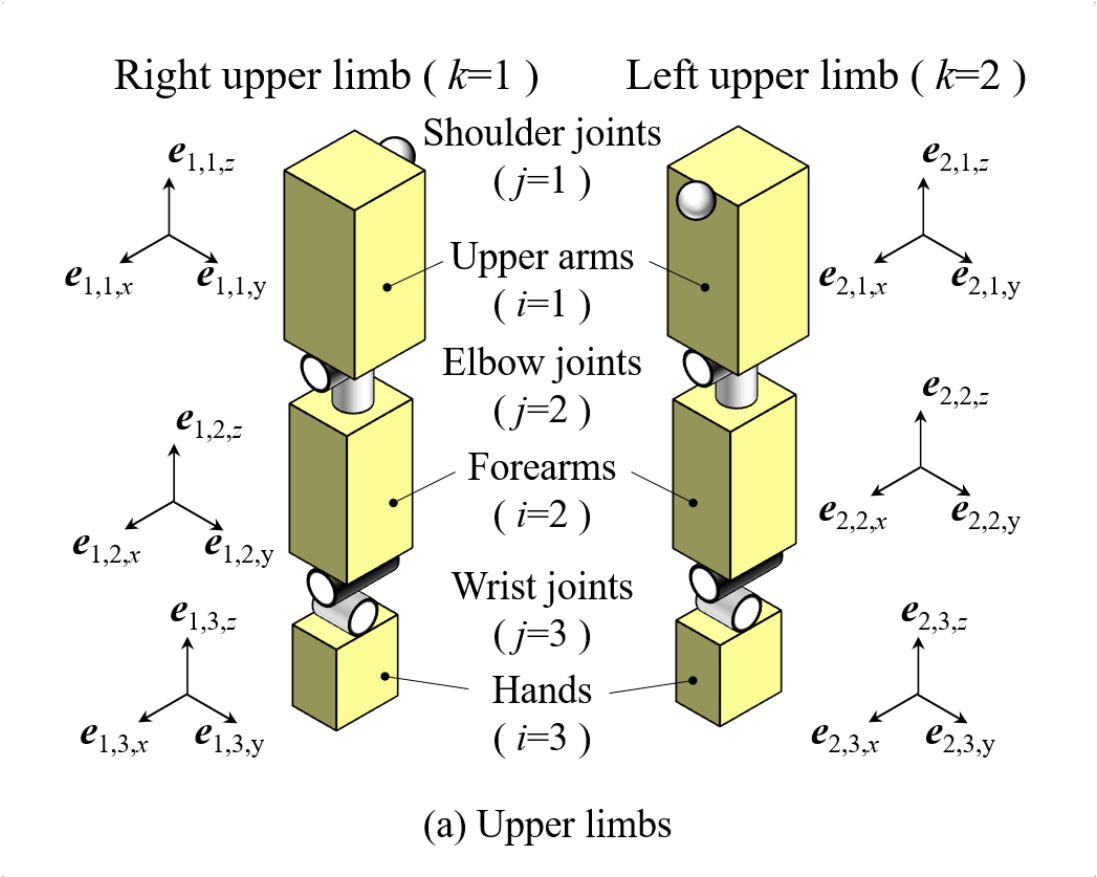

Figure 1. Schematic diagram for the 15-segment whole-body model.

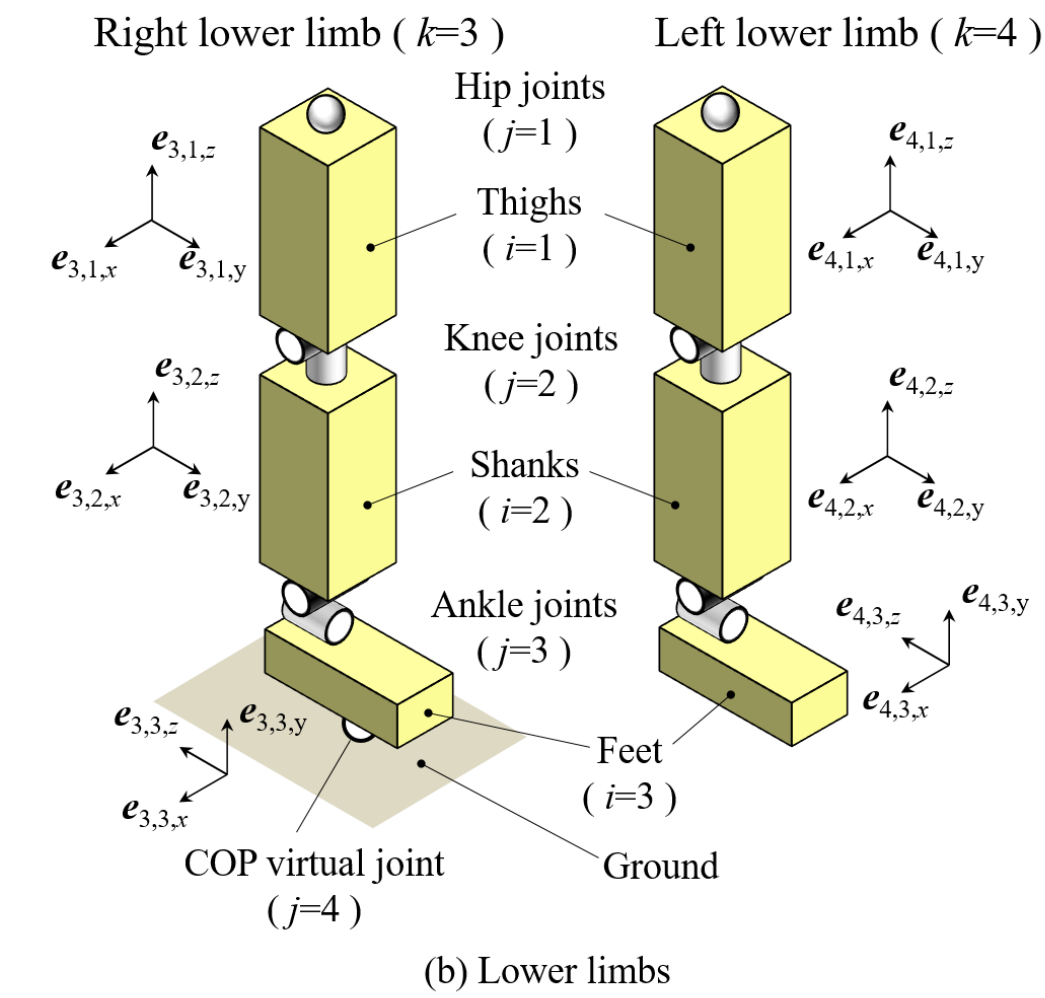

(b) Lower limbs

Figure 1 (cont.)

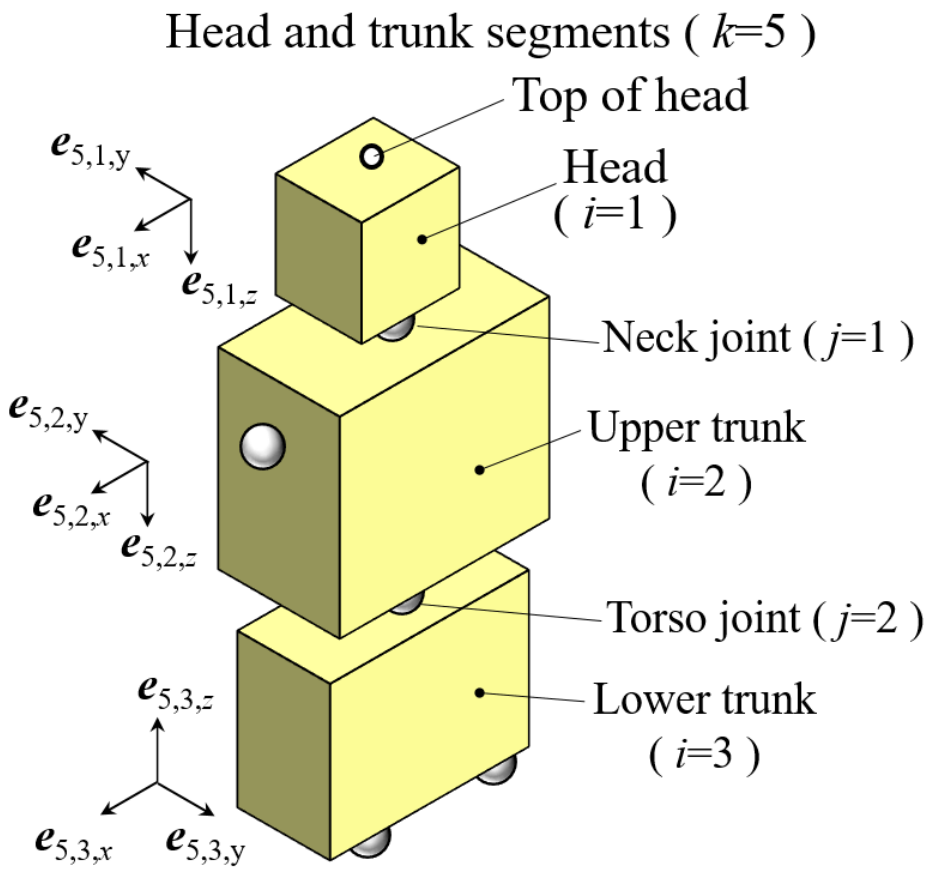

(c) Head and trunk

Figure 1 (cont.)

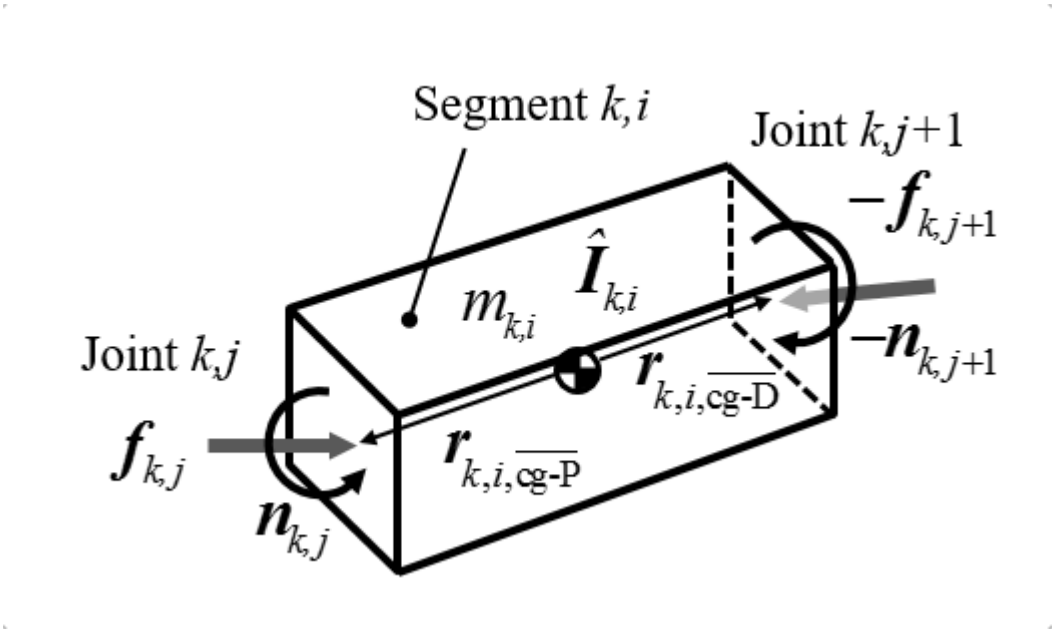

Figure 2. Free body diagram for segment *k,i*.

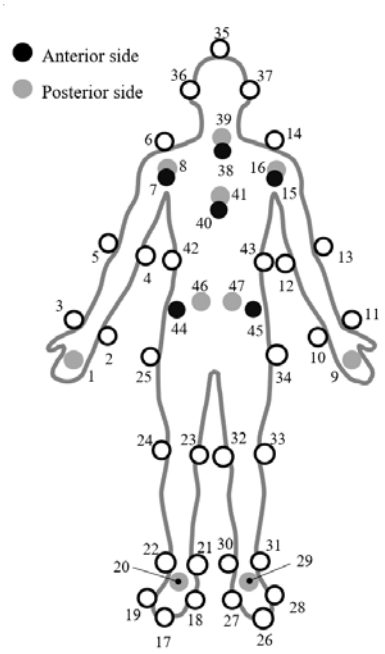

1: Head of the 3rd metacarpal of right hand
2: Medial aspect of right wrist
3: Lateral aspect of right wrist
4: Medial aspect of right elbow
5: Lateral aspect of right elbow
6: Right acromion
7: Anterior aspect of right shoulder
8: Posterior aspect of right shoulder

9: Head of the 3rd metacarpal of left hand
10: Medial aspect of left wrist
11: Lateral aspect of left wrist
12: Medial aspect of left elbow
13: Lateral aspect of left elbow
14: Left acromion
15: Anterior aspect of left shoulder
16: Posterior aspect of left shoulder

17: Right toe
18: 1st metatarsal bone of right foot
19: 5th metatarsal bone of right foot
20: Right heel
21: Right malleolus medialis
22: Right malleolus lateralis
23: Medial aspect of right knee
24: Lateral aspect of right knee
25: Right greater trochanter

26: Left toe
27: 1st metatarsal bone of left foot
28: 5th metatarsal bone of left foot
29: Left heel
30: Left malleolus medialis
31: Left malleolus lateralis
32: Medial aspect of left knee
33: Lateral aspect of left knee
34: Left greater trochanter

35: Vertex
36: Right tragus
37: Left tragus
38: Suprasternal notch
39: 7th cervical vertebrae
40: Xiphoid process
41: 10th thoracic vertebrae

42: Lower end of right rib
43: Lower end of left rib
44: Right anterior superior iliac spine
45: Left anterior superior iliac spine
46: Right posterior superior iliac spine
47: Left posterior superior iliac spine

Figure 3. Locations of the forty-seven reflective markers.

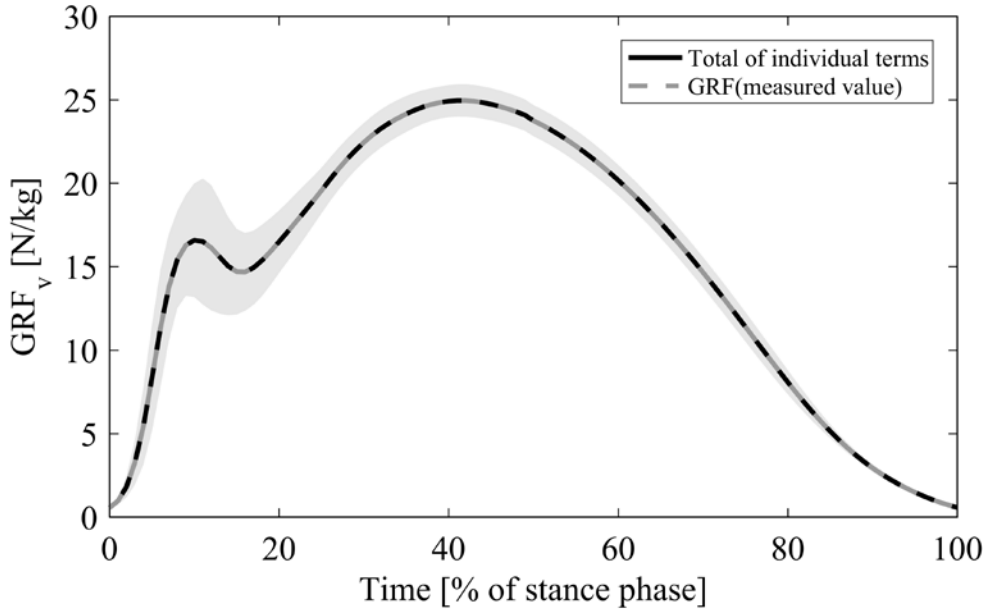

(a) Measured GRF and total of individual terms

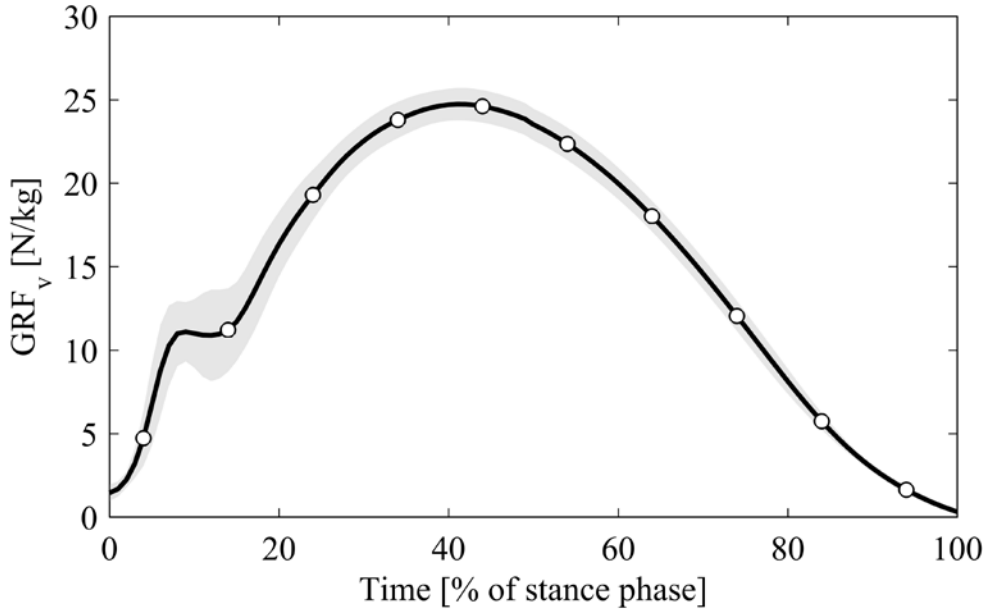

(b) Joint torque term

Figure 4. Contributions to the vertical ground reaction force, normalised to body mass and averaged across the participants at each normalised time. Each line represents the mean across the participants at each normalised time, and the shaded regions indicate one standard deviation either side of the mean.

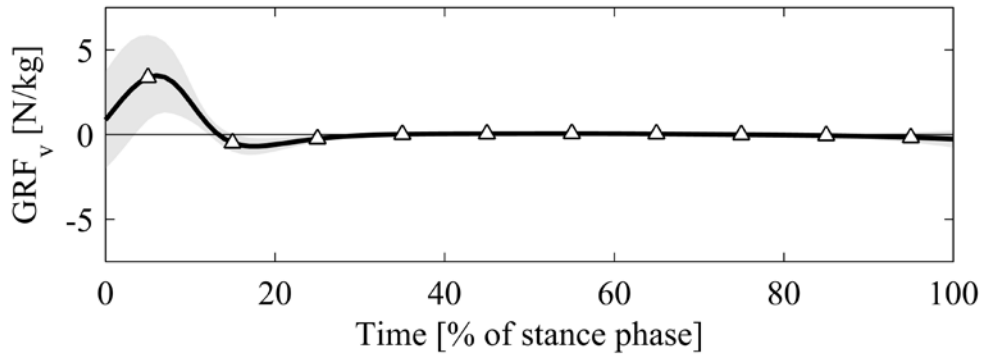

(c) Motion-dependent term

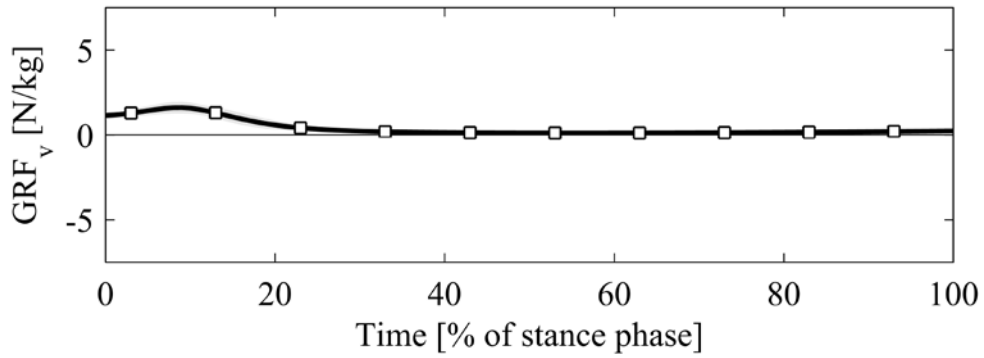

(d) Gravity term

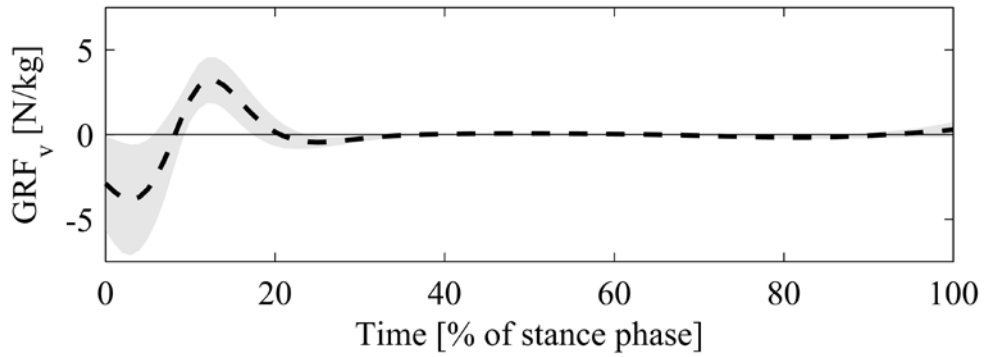

(e) Total of modelling error terms

Figure 4 (cont.)

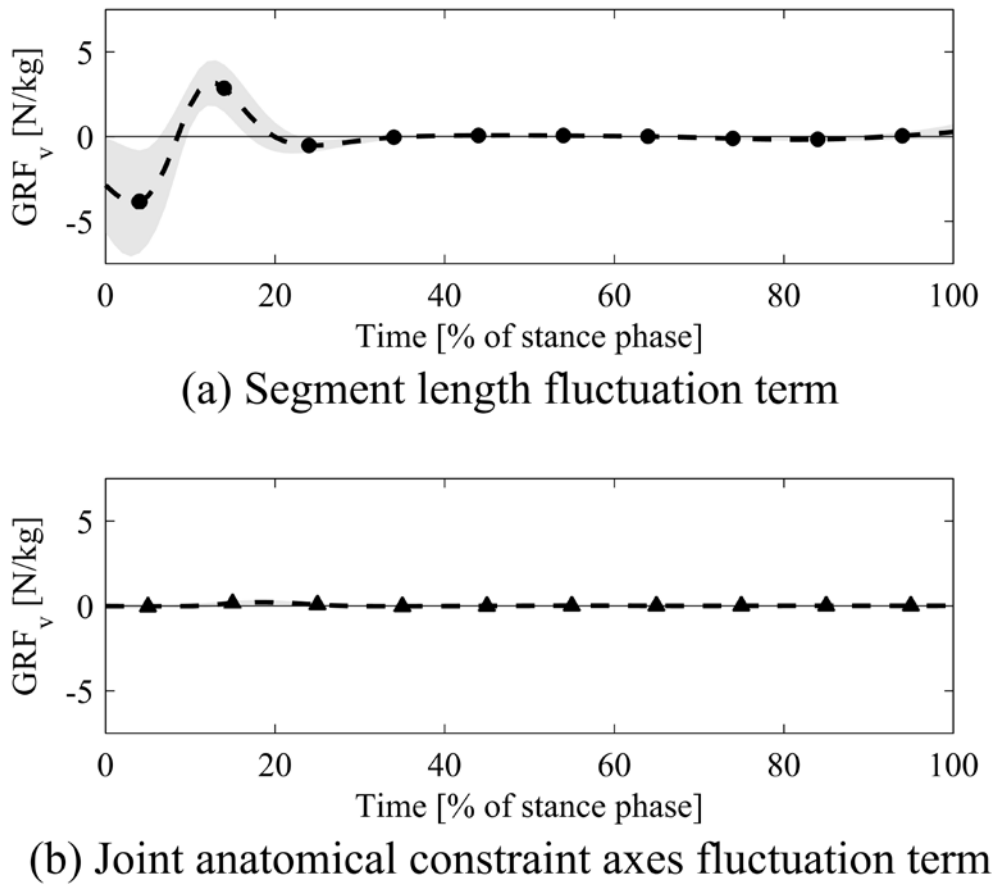

Figure 5. Contributions to the total modelling error for the vertical ground reaction force (seen in Figure 4e).

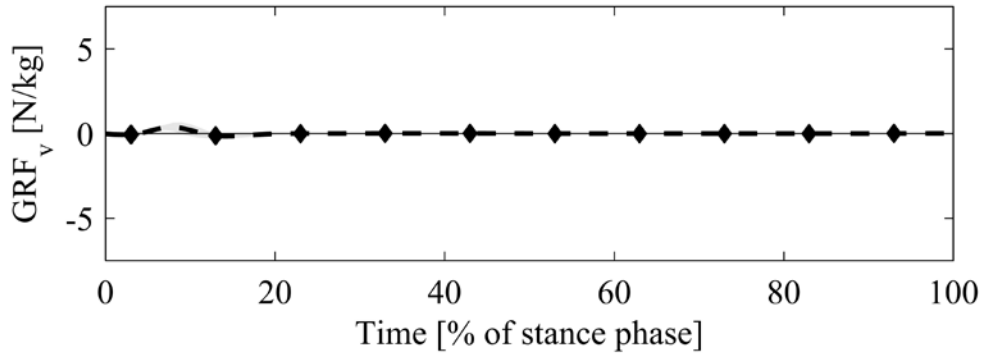

(c) Residual force error term

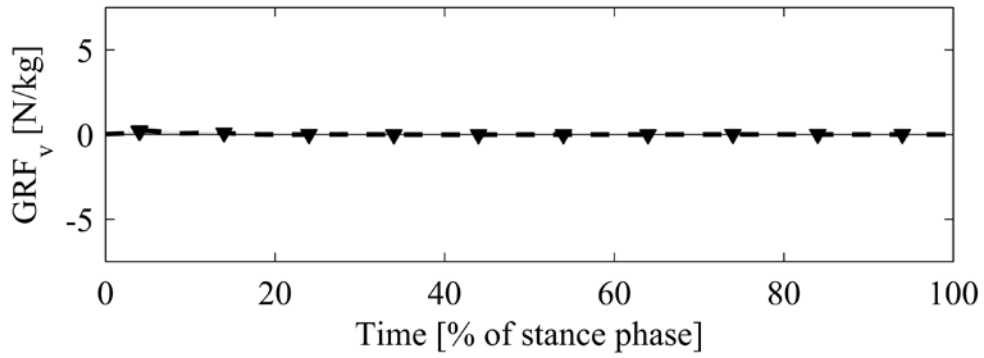

(d) Residual moment error term

Figure 5 (cont.)

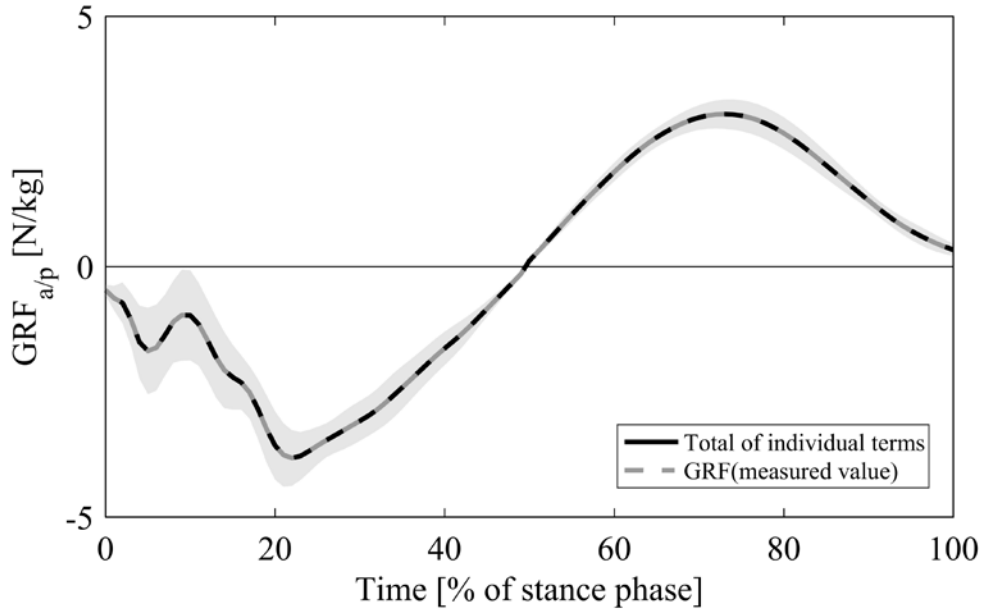

(a) Measured GRF and total of individual terms

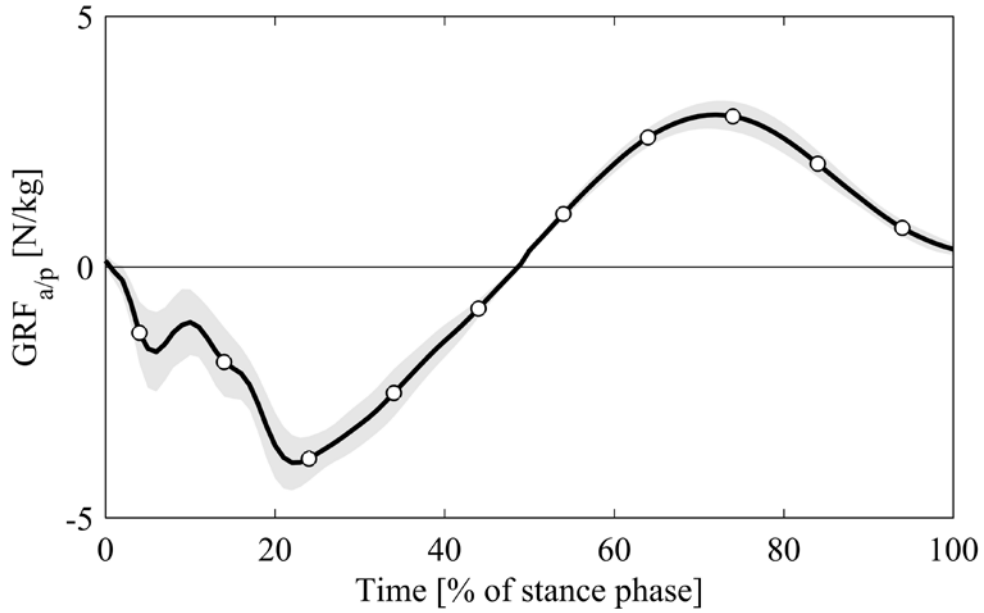

(b) Joint torque term

Figure 6. Contributions to the anterior/posterior ground reaction force, normalised to body mass and averaged across the participants at each normalised time. The shaded regions indicate one standard deviation either side of the mean.

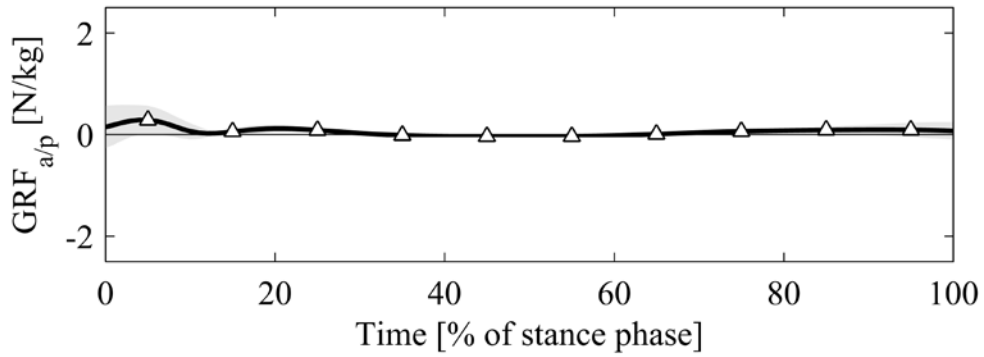

(c) Motion-dependent term

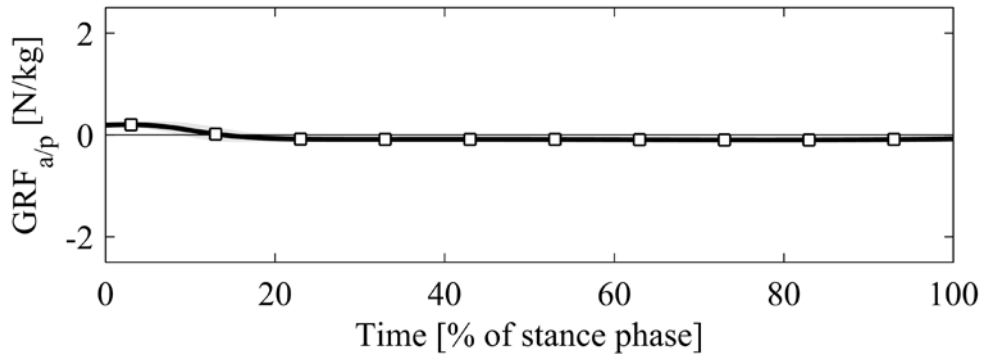

(d) Gravity term

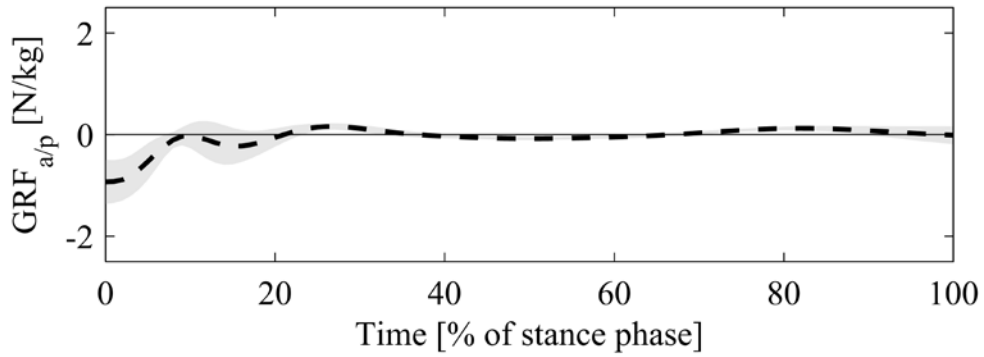

(e) Total of modelling error terms

Figure 6 (cont.)

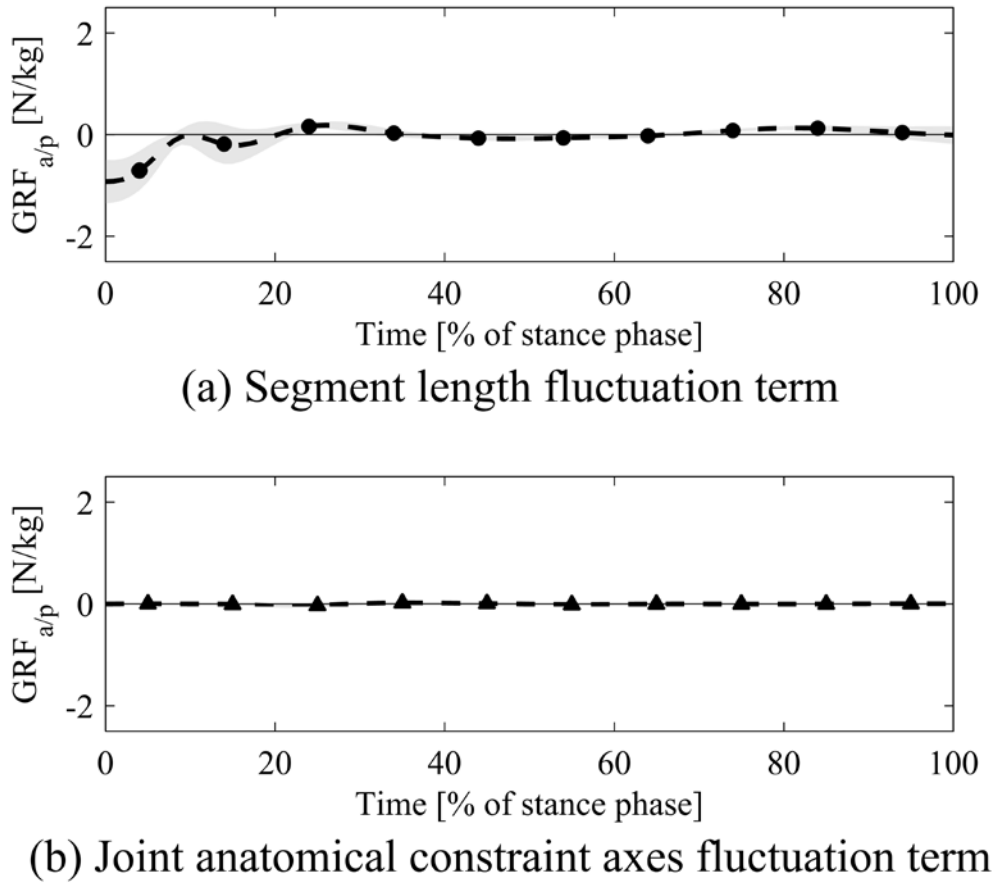

Figure 7. Contributions to the total modelling error for the anterior/posterior ground reaction force (seen in Figure 6e).

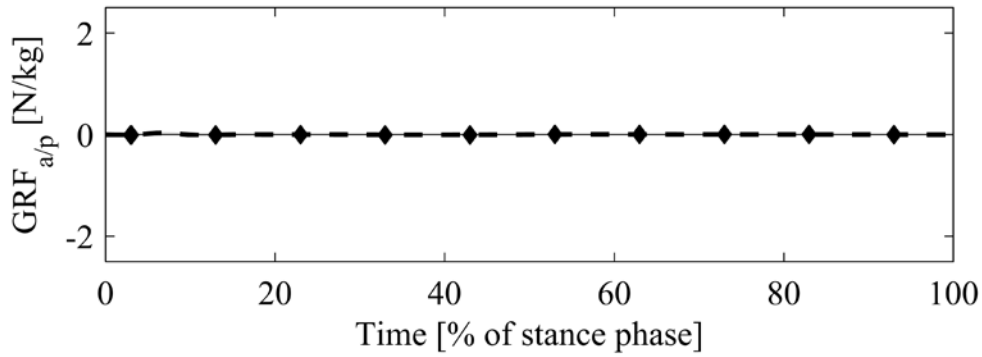

(c) Residual force error term

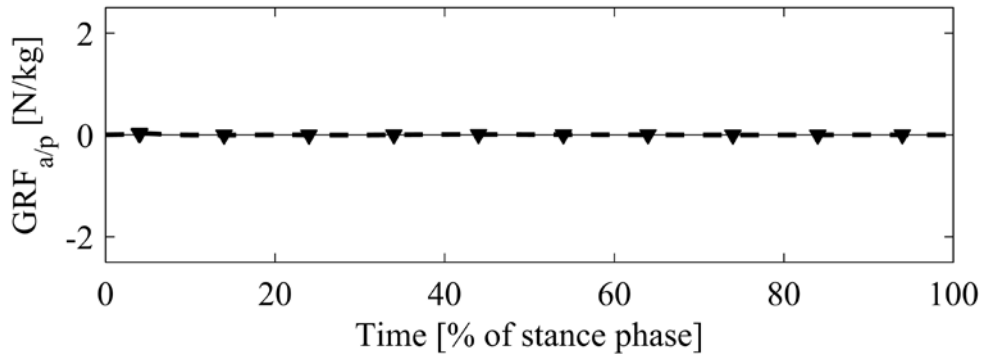

(d) Residual moment error term

Figure 7 (cont.)

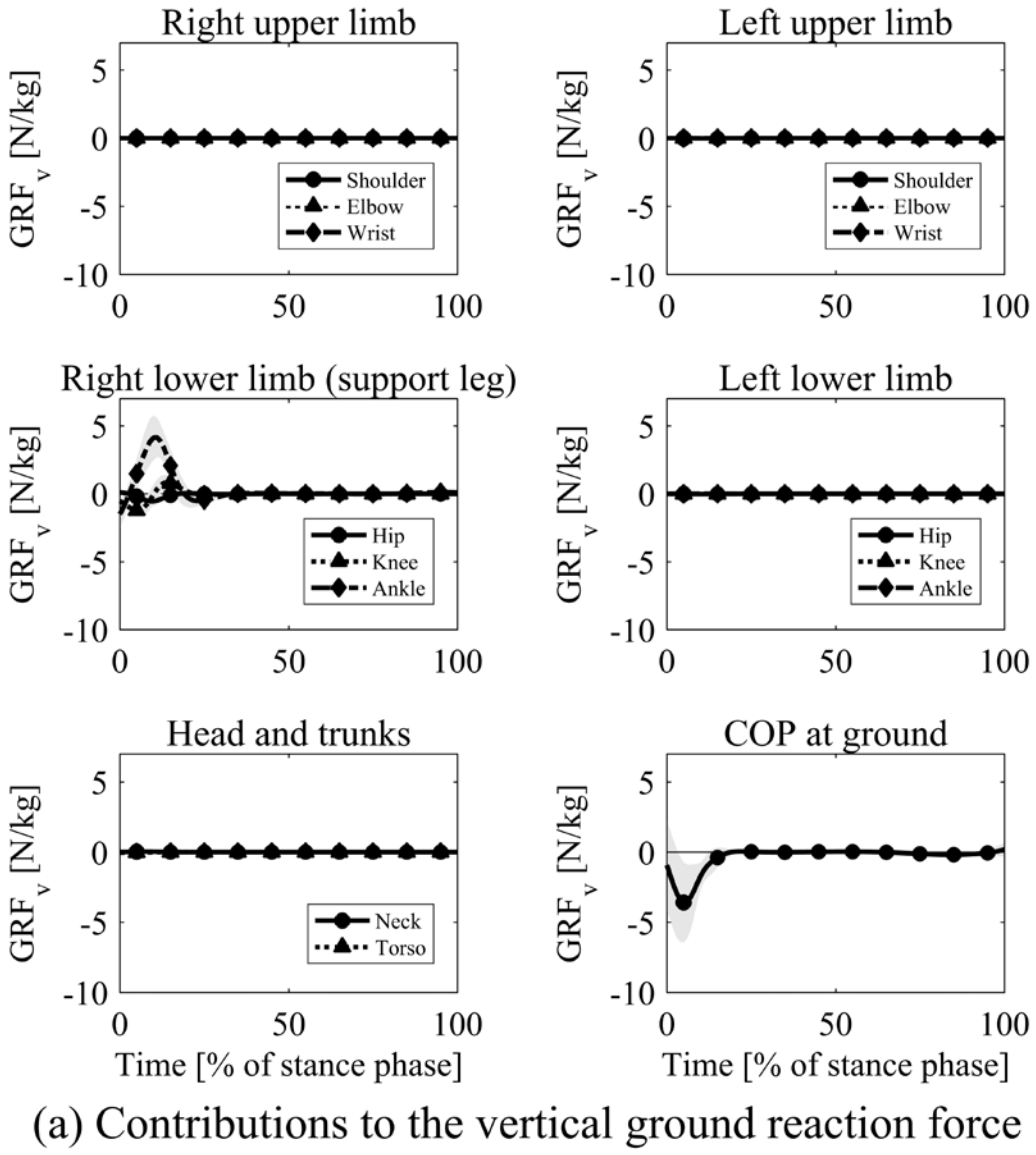

Figure 8. Contributions to the (a) vertical and (b) anterior/posterior components of the ground reaction force, normalised to body mass and averaged across the participants at each normalised time, from the segment length fluctuation term at each joint. The shaded regions indicate one standard deviation either side of the mean.

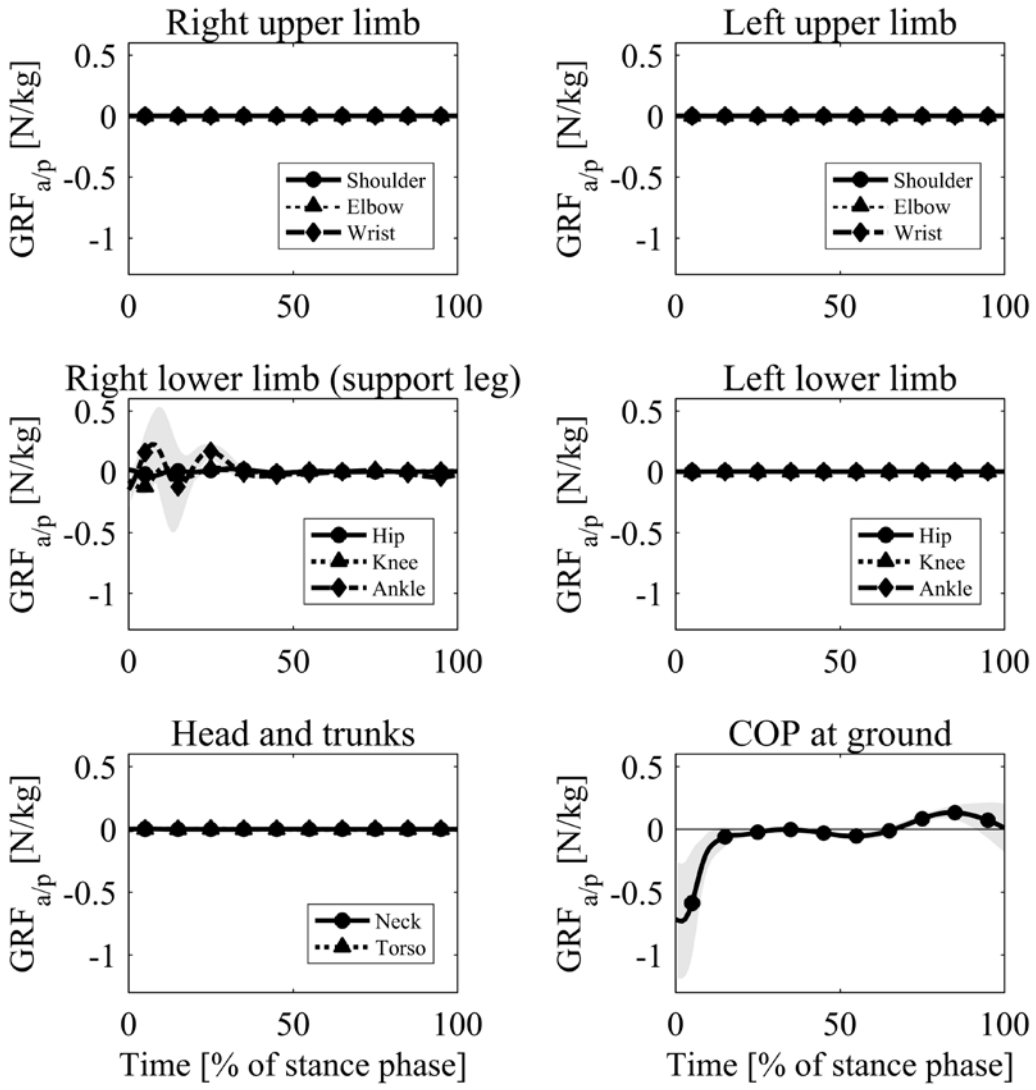

(b) Contributions to the anterior/posterior ground reaction

Figure 8 (cont.)

Table 1. The relative contribution arising from each error term (as a percentage of the average vertical and anterior/posterior ground reaction force over the course of stance phase) at different low-pass cut-off frequencies.

(a) Vertical ground reaction force

	Relative error contributions (%)			
Cut-off frequencies	5 Hz	15 Hz	25 Hz	50 Hz
Segment length fluctuation term	1.49 ± 0.63	4.34 ± 1.57	6.05 ± 1.98	6.73 ± 2.11
Joint anatomical constraint axes fluctuation term	0.05 ± 0.02	0.28 ± 0.08	0.38 ± 0.12	0.49 ± 0.17
Residual force error term	0.38 ± 0.15	0.24 ± 0.09	0.33 ± 0.11	0.42 ± 0.17
Residual moment error term	0.17 ± 0.07	0.17 ± 0.07	0.21 ± 0.10	0.32 ± 0.21

(b) Anterior/posterior ground reaction force

	Relative error contributions (%)			
Cut-off frequencies	5 Hz	15 Hz	25 Hz	50 Hz
Segment length fluctuation term	4.59 ± 1.02	7.91 ± 2.32	9.72 ± 2.66	11.01 ± 2.91
Joint anatomical constraint axes fluctuation term	0.15 ± 0.06	0.70 ± 0.27	0.92 ± 0.38	1.32 ± 0.61
Residual force error term	0.34 ± 0.13	0.32 ± 0.09	0.41 ± 0.12	0.54 ± 0.17
Residual moment error term	0.23 ± 0.11	0.28 ± 0.11	0.36 ± 0.16	0.57 ± 0.29